Climate Dynamics
https://doi.org/10.1007/s00382-023-07077-y

ORIGINAL ARTICLE

Impact of spring land-surface conditions over the Tibetan Plateau on the early summer Asian monsoon using an AGCM large ensemble

Hiroshi G. Takahashi[1] · Shiori Sugimoto[2] · Tomonori Sato[3]

Received: 20 September 2022 / Accepted: 18 December 2023

Abstract
Influence of land-surface memory effects over the Tibetan Plateau on the Asian summer monsoon has long been studied, but not quantified because of the difficulty of extracting only these effects from observational data. This study examines the impact of spring land-surface conditions, including surface air temperature (SAT) and snow cover, over the Tibetan Plateau and its surrounding regions on the early stage of the Asian summer monsoon using large-ensemble experiments produced by an atmospheric global climate model (AGCM). The results show that the above-normal SAT over and around the Tibetan Plateau in May can enhance June monsoon circulation without the sea surface temperature (SST) forcing. The physical mechanism behind this involves warmed surface air over the plateau enhancing the north–south SAT gradient, leading to strengthening the Asian summer monsoon circulation and precipitation. Inter-ensemble correlation analysis indicated that SAT warming over the plateau is clearly associated with upper-tropospheric anti-cyclonic circulation anomalies in May. Also, although winter land-surface signals do not persist until late spring, SAT anomalies in March tend to persist until May, explaining 10–20% of the total SAT variance in May. Interestingly, the spring SAT impacts on June monsoon circulations vary interannually, indicating that the contribution of the land–atmosphere (L–A) coupling process to interannual monsoon variability differs from year to year. Active L–A coupling years tend to coincide with cooler SSTs with anomalous low-level divergence and upper-level convergence over and around the Maritime continent, implying that SST forcing is associated with the L–A coupling strength. Specifically, in May of the developing stage of monsoon circulation, the weak Walker circulation over the equatorial and northern Indian Ocean and undeveloped monsoon circulation are suitable for the L–A coupling to influence the development of the monsoon circulation effectively. However, the well-known oceanic events, such as El Ni$\tilde{n}$o, are found to be less connected with the interannual L–A coupling variations.

Keywords Surface air temperature · Asian monsoon · AGCM · Large-ensemble experiment

1 Introduction

Land-ocean thermal contrasts in the troposphere drive Asian monsoon systems. The thermal contrast is the most prominent near the surface, and it changes seasonally. In the spring and early summer, the Eurasian landmass including the Tibetan Plateau is dramatically heated. In contrast, sea surface temperatures (SSTs) in adjacent oceanic regions warm up more slowly because of a large thermal capacity of sea water (e.g., Loschnigg and Webster 2000). The thermal contrast between the Eurasian continent, including the Tibetan Plateau, and adjacent oceanic regions is a key to determine the seasonal march of the Asian monsoon (Yanai and Wu 2006; Yang and Lau 2006; Yasunari 2006).

Recently, many studies have reported that the thermal contrast between the northern and southern hemispheres due to the moist static energy gradients associated with the seasonal swing of solar irradiance can also be an essential components of the conceptual view for the large-scale monsoon circulation (Trenberth et al. 2000; Zhou and Xie 2018; Hill 2019; Geen et al. 2020; Chen et al. 2022). Some researchers suggested that monsoon circulation can be generated even without the land-ocean distribution (Zhou and Xie 2018;

✉ Hiroshi G. Takahashi
hiroshi3@tmu.ac.jp

[1] Tokyo Metropolitan University, 1-1 Minamioosawa, Hachiooji 193-0397, Tokyo, Japan

[2] Japan Agency for Marine-Earth Science and Technology, Yokohama, Kanagawa, Japan

[3] Faculty of Environmental Earth Science, Hokkaido University, Sapporo, Hokkaido, Japan

Published online: 20 January 2024

Seth et al. 2019; Geen et al. 2020). Also, the importance of interhemispheric thermal contrast in large-scale monsoon circulation has recently been discussed as a response to variations of anthropogenic aerosol loading (e.g., Wang et al. 2019; Takahashi et al. 2018). However, realistic regional monsoon circulations should emerge with topography (e.g., Boos and Kuang 2010), although the role of topography in the regional monsoon circulations is complex.

Over the past few decades, the roles of the dynamical and thermodynamic effects of the Tibetan Plateau and the surface conditions of the Eurasian continent on Asian monsoon circulation and precipitation have been widely studied (e.g., Wu et al. 2007; Boos and Kuang 2010; Wu et al. 2012). As a potentially important factor in the interannual variability and seasonal predictions of the Asian monsoon, the snow cover of the Tibetan Plateau controls the strength of the Indian or broad Asian monsoons, as shown by statistical and dynamical analyses of observational datasets and numerical experiments (Hahn and Shukla 1976; Yasunari et al. 1991; Vernekar et al. 1995). The strength of Asian monsoons can also vary interannually, resulting largely from the interannual variability in oceanic conditions (Lau and Wang 2006; Yang and Lau 2006).

In linkage with global climate variability, such as El Ni$\tilde{n}$o-Southern Oscillation (ENSO), many studies have investigated the impact of snow cover over the Tibetan Plateau on the Asian monsoon and global climates (e.g., Shaman and Tziperman 2005). Additionally, observational studies have examined the relationships between land-surface conditions before summer, such as surface air temperature (SAT) and snow cover, and the Asian monsoon in summer (Bamzai and Shukla 1999; Kripalani et al. 2003; Wu and Qian 2003). In short, pre-summer low SATs with broad snow cover over the Tibetan Plateau are associated with mid-summer weak monsoon circulation and decreased precipitation. This relationship is considered due to the weaker north–south SAT gradient (Goswami and Xavier 2005). The effects of land-surface conditions further alter the monsoon onset (Yanai et al. 1992). The weaker north–south SAT gradients as mentioned above are associated with both low SAT anomalies over the Tibetan Plateau and regions to the west, as well as warm SAT anomalies over South and Southeast Asia, which tend to occur during El Ni$\tilde{n}$o conditions. Therefore, it is crucial to consider the effects of both land and ocean when monsoon variability is investigated.

In the observational datasets, however, it is difficult to understand the impacts of land-surface conditions on Asian monsoon because the impact of SST anomalies on Asian monsoon is relatively more prominent than that of the land-surface conditions (e.g., Webster et al. 1999). To investigate the role of the land-surface conditions on the Asian monsoon climate, we analyze the internal climate variability in a land–atmosphere (L–A) system under common SST conditions, thereby eliminating the effects of SST anomalies. Another challenge of analyzing observational datasets for this purpose is insufficient sample years of similar anomalous SST conditions; for instance, number of El Ni$\tilde{n}$o years are limited for robust statistical analysis (e.g., Kumar et al. 1999).

To investigate the role of land-surface conditions under the same SST conditions, one solution is the utilization of ensemble experiment by an atmospheric global climate model (AGCM) with a prescribed observed SST anomaly. In general, AGCMs cannot faithfully capture the atmosphere–ocean coupling processes, but realistic observed SST anomalies can be prescribed. Also, the number of experiments with different initial conditions can produce a variety of internal climate variability in the L–A systems. A more detailed discussion of the differences between forced responses and internal climate variability based on global climate model (GCM) large-ensemble experiments (LEns) can be found in Kay et al. (2015).

LEns by AGCM with the prescribed observed SST anomaly (LEns-AGCM) is useful to distinguish SST-forced responses and internal climate variability within the complex interannual variation of the Asian monsoon. Accordingly, the present scientific question can be addressed using the LEns-AGCM. Recently, there has been a growing trend toward the use of LEns for multiple research purpose (e.g., Murray et al. 2020).

Recently, Xue et al. (2021; Impact of Initialized Land Temperature and Snowpack on Sub-seasonal to Seasonal Prediction; LS4P project) and related studies (e.g., Diallo et al. 2022) addressed the impacts of surface hydrometeorology over the Tibetan Plateau, including snow cover, on extreme weather events over Asian monsoon regions and the global domain. Because heavy precipitation and related disasters in East Asia have recently increased (Takahashi and Fujinami 2021), the predictability of extreme weather events is an urgent issue. LS4P multi-model experiments have proposed the effects of land-surface conditions on Asian monsoon climates (e.g., Diallo et al. 2022). The LS4P project mainly focuses on specific years in which severe extreme events occurred in the region. Thus, interannual differences in the impacts of land-surface conditions need to be characterized.

To this end, the present study focuses on the impact of land-surface conditions on the early summer Asian monsoon, particularly in May and June. This is because the effects of land-surface conditions over the Eurasian continent on the Asian monsoon are dominant in spring and early summer since snow cover mostly vanishes by May. In addition, the different interannual variations between early and late summer (e.g., Ailikun and Yasunari 2001) might be correlated to the complex non-linear effects associated with the tropical cyclones seasonally developing over the Southeast Asian monsoon and western North Pacific

monsoon regions in late summer (Takahashi and Yasunari 2006, 2008).

Thus, the primary purpose of this study is to quantitatively understand the impacts of spring land-surface conditions, including snow cover, on the Asian monsoon circulation strength in early summer under the same SST conditions. This study uses an LEns-AGCM dataset. Although the mechanism of the land-surface impact on the Asian summer monsoon has been suggested, its contribution is yet to be quantified because of the presence of oceanic impact, which also has great impact, and difficulties to separate from each other. Thus, in this study, we quantify the land-surface impact, simulated as internal climate variability in an L–A system. Finally, the conditions under which land-surface impacts become dominant are also considered. The remainder of the text is structured as follows: Sect. 2 presents the datasets and methods used. Section 3 clarifies the differences between SST-forced responses and internal L–A climate variability, and the impacts of land-surface conditions on the Asian monsoon. Section 4 discusses the persistence of land-surface memory and predictability in a specific year, and Sect. 5 presents the conclusions.

2 Datasets and methods

2.1 Datasets

To investigate the impact of land-surface conditions, we mainly use Atmospheric Model Intercomparison Project (AMIP)-type LEns, referred to as LEns-AGCM. We selected the 100-ensemble experiment dataset of the Database for Policy Decision-Making for Future Climate Change (d4PDF; Mizuta et al. 2017, http://www.miroc-gcm.jp/~pub/d4PDF/index_en.html), which used a 60-km AGCM mainly developed at the Japan Meteorological Agency/Meteorological Research Institute (JMA/MRI). We use the historical experiment of d4PDF. For historical experiments of d4PDF, the prescribed SSTs were observed SSTs with small random perturbations added. The detailed configuration and basic performance of the AGCM and datasets can be found in Mizuta et al. (2017) and on the webpage above. We use the period from 1979 to 2011. To understand the relationship between the June Asian monsoon circulation and the pre-June months land-surface condition, we mainly use June and pre-June months (March–April–May) data. From the d4PDF datasets, variables of SAT, surface temperature (not air), snow cover, precipitation, horizontal winds at 850 and 200 hPa, downward and upward shortwave radiations at the surface, and total cloud cover are analyzed. All the variables are obtained as monthly average value.

In the d4PDF historical experiment, SSTs were prescribed as boundary conditions, indicating that oceanic forcing is treated as external forcing. On the other hand, the land surface is coupled with the atmosphere without any assimilation processes, meaning that the L–A interaction is regarded as an internal process.

To evaluate the reproducibility of the interannual variation in Asian monsoon circulation and SAT of d4PDF, the Japanese 55-year Reanalysis Project (JRA-55; Kobayashi et al. 2015; http://jra.kishou.go.jp/JRA-55/index_en.html) dataset is employed, including the horizontal winds at the 200-hPa and 850-hPa levels, and SAT. The horizontal resolution of JRA-55 is 1.25°, and we use only the period from 1979 to 2011. In addition, to check the seasonal march of snow cover, the Northern Hemisphere EASE-Grid Weekly Snow Cover and Sea Ice Extent (Brodzik and Armstrong 2013) with a spatial resolution of 1° of Northern Hemisphere is used from 1979 to 1995. Despite being somewhat overestimated, the overall patterns can be reproduced by d4PDF through a comparison of d4PDF climatology and observations over the same period (figure not shown). To investigate interannual variations in SST, we use the Centennial in situ Observation-Based Estimates SST (COBE-SST; Ishii et al. 2005), which is equivalent to the prescribed SST values in d4PDF. This global monthly dataset has a spatial resolution of 1°. The ENSO indices used here follow the definitions of the Japan Meteorological Agency (https://ds.data.jma.go.jp/tcc/tcc/products/elnino/ensoevents.html).

Furthermore, SAT, surface temperature, and snow cover are used as variables to represent land-surface conditions. We confirmed that their variables are highly correlated on the monthly time-scale. This result indicates that SAT and surface temperature include the effects of snow cover on the monthly time-scale. The results of Sect. 4.1, to what extent the early spring (March) land-surface condition can explain late spring (May) SAT, are similar even if composite and variance analyses based on surface temperature are replaced with snow cover (see also Sect. 4.1).

2.2 Methods

To understand the L–A internal variability in the Asian monsoon system, we separately analyze the d4PDF data for each year, namely the LEns-AGCM experiment under the same prescribed SSTs. One hundred ensemble members are available to understand the relationship between surface conditions and monsoon activity under the same SSTs.

The strength of the South and Southeast Asian monsoon circulation is quantified using the major Asian monsoon index (Webster and Yang 1992; MI). MI is calculated as the difference between the lower and upper-tropospheric zonal winds ($u850 - u200$), which are averaged over EQ–20°N, 40°E–110°E. Both low-level westerlies and upper-level easterlies contribute to an increased MI. A higher MI indicates stronger monsoon circulation (in units of m s^{-1}).

To analyze the internal climate variability of the Asian monsoon system in d4PDF, inter-ensemble correlation and regression maps [$Corr_{inter-ens}(i,j)$, see Eq. (1)] are created based on MI. Simultaneous or time-lag inter-ensemble correlations and regressions can be calculated for a specific period for each year. For example, the simultaneous relationship between June MI and June SATs under the SST conditions of June 1979 can be explored. Here, we have SATs for all global grids, and MI is a time-dependent area-averaged value. Using 100 ensemble members, we can calculate the inter-ensemble correlation between SATs and MI, using Eq. (1).

$$Corr_{inter-ens}(i,j) = \frac{\sum_{e=1}^{100}(MI_e - \overline{MI})(SAT_e(i,j) - \overline{SAT(i,j)})}{\sqrt{\sum_{e=1}^{100}(MI_e - \overline{MI})^2 \sum_{e=1}^{100}(SAT_e(i,j) - \overline{SAT(i,j)})^2}} \quad (1)$$

where i and j are longitude and latitude grid numbers, respectively. $\sum_{e=1}^{100}$ is the sum of the 100 ensemble values, and the overbar denotes the 100-ensemble mean. The statistical significance of the inter-ensemble correlations was determined at the 99% level based on 98 degrees of freedom. Inter-ensemble regression can be computed using a formula similar to Eq. (1) (the formula is omitted).

The same formula as Eq. (1) can be used for other indices, such as area-averaged SAT. To quantify the *L–A* coupling strength index, we additionally use an averaged SAT over the Tibetan Plateau and its surrounding regions (28° N–40°N, 60°E–100°E), which is discussed in Sects. 3 and 4. The area-averaged SAT the Tibetan Plateau and its surrounding regions is referred to as SAT_{TP}. Also, the time-lag relationships between the June MI and SATs in May under common SST conditions can be examined and the results are reported in Sect. 3.2.

3 Results

3.1 SST controlling variability and the internal climate variability in the land–atmosphere system: reproducibility of interannual variations

We first exmiane the interannual variations of the Asian monsoon indicated by MI simulated by d4PDF (Fig. 1). Generally, MI values are closely associated with ENSO phases. Although discussion of whether ENSO can clearly explain the interannual variation of the Asian monsoon is beyond the scope of the present study, the observed time-series of June MI (Fig. 1a) shows that weaker Asian monsoon years correspond to El Niño and post El Niño years (e.g., 1983, 1992, 1997, and 2009), whereas stronger monsoon years correspond to La Niña years (e.g., 1984, 1985, 1999, and 2010). Actually, the correlation coefficient between June MI and Niño 3 SST in April–June is −0.51 ($p = 0.0025$). These observed variations in the Asian monsoon, however, should include the response of monsoon to SST forcing, internal land–atmosphere climate variability, and other processes. Thus, it is generally difficult to distinguish the impacts of land-surface conditions from other driving factors.

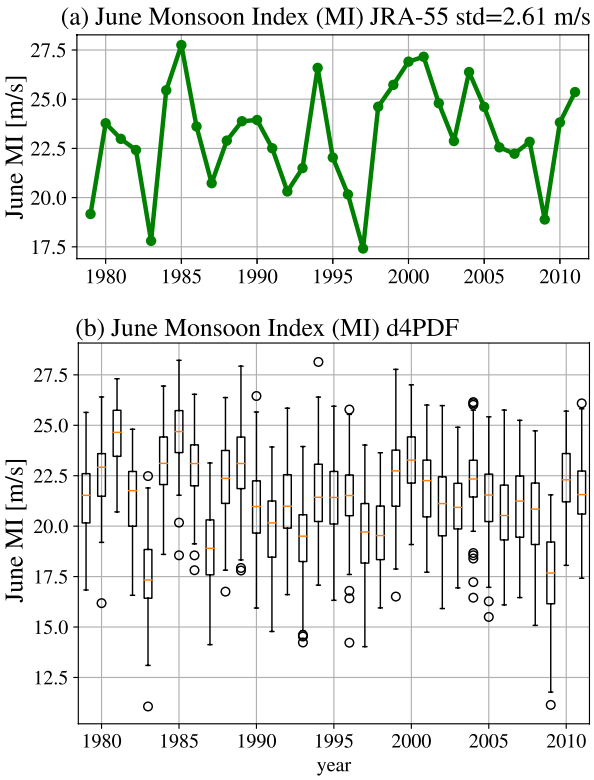

Fig. 1 Time-series of monsoon index (MI) in June calculated by the Japanese 55-year Reanalysis (JRA-55; upper panel). Boxplot of simulated MIs in June from the Database for Policy Decision-Making for Future Climate Change (d4PDF; lower panel)

Here, Fig. 1 shows the time-series of the median of the simulated MI are similar to the observation, implying that d4PDF can reproduce the observed interannual variation in MI. The ensemble mean values represent the impact of external forcing because the effects of internal climate variability among the 100 members are canceled. Thus, the simulated ensemble mean MI can be explained by SST forcing in the LEns-AGCM framework. Because both the observed and median values of the simulated members are related to the SST anomalies, it is reconfirmed that SST forcing is one of the drivers of interannual MI variation. We will quantify this later.

To understand the impacts of the land-surface conditions on the early-summer monsoon circulation, the land-surface conditions during the transition from spring to summer are investigated. In addition, we will show that May SATs over and around the Tibetan Plateau are related to the June MI (Sect. 3.2).

The observed SAT_{TP} time-series is weakly correlated with ENSO events (Fig. 2a), because low SAT_{TP} years correspond to El Ni$\tilde{n}$o years (e.g., 1982, 1987, 1992, and 2009), and warm years correspond to La Ni$\tilde{n}$a years (e.g., 1984, 1995, and 2010). The correlation coefficient between May SAT_{TP} and Ni$\tilde{n}$o 3 SST in April–June is −0.36 ($p = 0.042$). SST forcing to May SAT_{TP} is found but relatively weaker than that to MI, which will be validated later as percentage variance.

The d4PDF simulated time-series of the SAT_{TP} are similar to the observed SAT_{TP} for each year, particularly the median values (Fig. 2b), which are also similar to MI. This result suggests that SST forcing can partly control the interannual variability in SAT_{TP}.

The amplitude of the interannual variation in June MI in d4PDF is also examined here. In d4PDF, the standard deviation of the interannual June MI is also calculated for each member. The observed interannual standard deviation of June MI in JRA-55 σ_{MI-obs} is 2.61 m s^{-1}, whereas the median value of the interannual standard deviation among the 100 members $\widetilde{\sigma}_{MI-sim}$ is 2.46 m s^{-1}, which is close to the observed value. This result indicates that the amplitude of the interannual variations in MI is simulated by d4PDF.

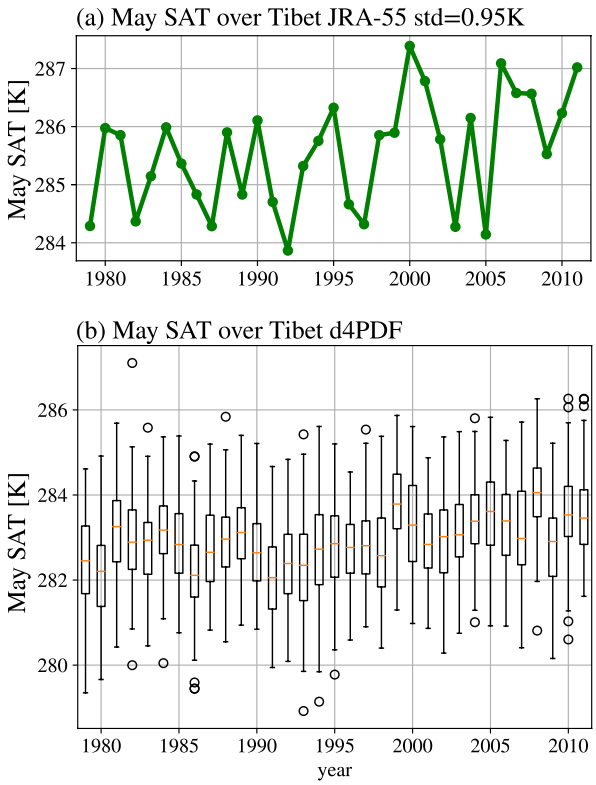

Fig. 2 Time-series of SAT_{TP} in May calculated by JRA-55 (upper panel). Boxplot of simulated SAT_{TP} in May from d4PDF (lower panel). The observed and simulated SAT_{TP} were averaged SATs over the Tibetan Plateau and its surrounding regions (28°N–40°N, 60° E–100°E)

In addition, the extent to which SST-forcing explained the interannual variance of MI is estimated using percentage variance. Here, the interannual standard deviation of the median MI value $\sigma_{MI-sim-SST}$ is 1.66 m s^{-1}, regarded as the magnitude of SST-forced interannual variation of MI. $\sigma_{MI-sim-SST}$ is first chosen as the median for each year from the 100 ensemble members, and a single standard deviation is then calculated (a single time-series of the median values of the boxplot in Fig. 1b). Using the percentage variance of SST-forcing, given as $\sigma^2_{MI-sim-SST}/\widetilde{\sigma}^2_{MI-sim}$, it is estimated that approximately 41% of the total variance of MI is controlled by SST forcing. Thus, SST forcing is the major driver of interannual MI variation.

Next, the amplitude of the interannual variation in May SAT_{TP} is examined in d4PDF. The observed value of the interannual standard deviation in SAT_{TP}, $\sigma_{SAT-obs}$ is 0.95 K, whereas the median value of the simulated interannual standard deviation in SAT_{TP}, $\widetilde{\sigma}_{SAT-sim}$ is 1.09 K, which implies that the amplitude of the interannual variation is reasonably simulated in d4PDF.

Similarly, the SST-forced variance in May SAT_{TP} is assessed using the percentage variance $\sigma^2_{SAT-sim-SST}/\widetilde{\sigma}^2_{SAT-sim}$. SST forcing explains approximately 18% of the SAT_{TP} variance considering that the interannual standard deviation in the median SAT_{TP} values $\sigma_{SAT-sim-SST}$ is 0.46 K. Thus, SST forcing has less effect on the May SAT_{TP} variability than on the June MI, which implies that internal climate variability is more dominant in the SAT_{TP} variability than in the June MI variability. This result may reflect the fact that SST forcing is limited to inland regions and weak over mid-latitudes due to the chaotic nature of the atmosphere that dampens the signal from the ocean. With the reasonable reproducibility of the Asian monsoon and the related SAT variability in d4PDF, the following sections investigate the relationship between land-surface conditions and monsoon circulations.

3.2 Impact of land-surface conditions on summer monsoon circulation

Here, we delve into the inter-ensemble correlation between the Asian monsoon circulation in June and pre-June SATs to investigate the impacts of spring land-surface conditions on early summer monsoon circulation. For a selected target year, the inter-ensemble correlation indicates if the SATs of the pre-June month can statistically explain the Asian monsoon circulation in June. Each year, the time-space characteristics of land-surface conditions that intensify the monsoon circulations are explored. Below, a case study of 1995, a year with a notable inter-ensemble correlation between June MI and May SATs (referred to as *active L–A* year), is shown. The results for the other years are presented and discussed in subsequent sections.

3.2.1 Case study: 1995

The year 1995 is selected as the target year for the case study. The ENSO phase was neutral this year, implying that the SST forcing may not have been substantial. Simultaneous relationships between June MI and June 850-hPa winds and precipitation show enhanced low-level monsoon westerlies and precipitation over the South and Southeast

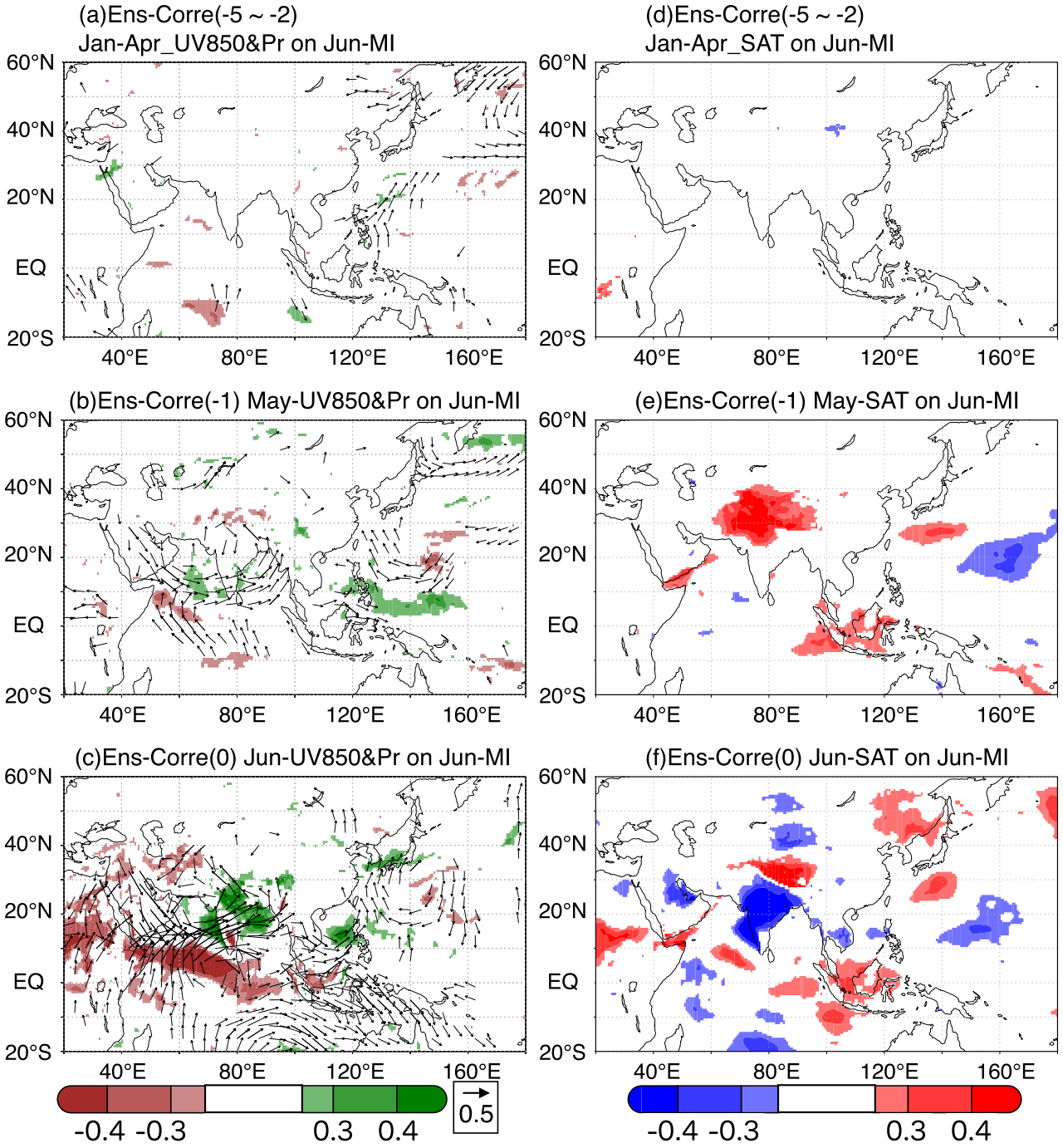

Fig. 3 Inter-ensemble correlation map between June MI and (a–c) low-level circulations (vectors) and precipitation (colors), and (d–f) SATs in 1995. **a, d** denotes lag-inter-ensemble correlation map between June MI and the variables averaged from January to April. **b, e** is lag-inter-ensemble correlation map between June MI and the variables in May. **c, f** denotes simultaneous inter-ensemble correlation map between June MI and the variables in June. All plotted correlations were statistically significant at $p < 0.01$ (two-tailed Student's t test)

Asian monsoon regions (Fig. 3c), indicating that this inter-ensemble correlation method could be useful, as expected. We then move on to analyze the lagged inter-ensemble correlation between June MI and May SATs. A systematic positive correlation is found over the Tibetan Plateau and its surrounding regions, implying that May's warm land-surface conditions can enhance the June MI values. We further verified the inter-ensemble correlation between June MI and land-surface conditions, as well as June MI and atmospheric circulations from January to May, and found statistically significant lagged inter-ensemble correlations only in May (Fig. 3). The signals are weak or negligible from January to April (Fig. 3a, d). Lagged inter-ensemble correlations between June MI and snow cover from January to April also show no statistically significant signals (not shown), suggesting that the influence of land-surface conditions in winter and early spring on June MI is weak.

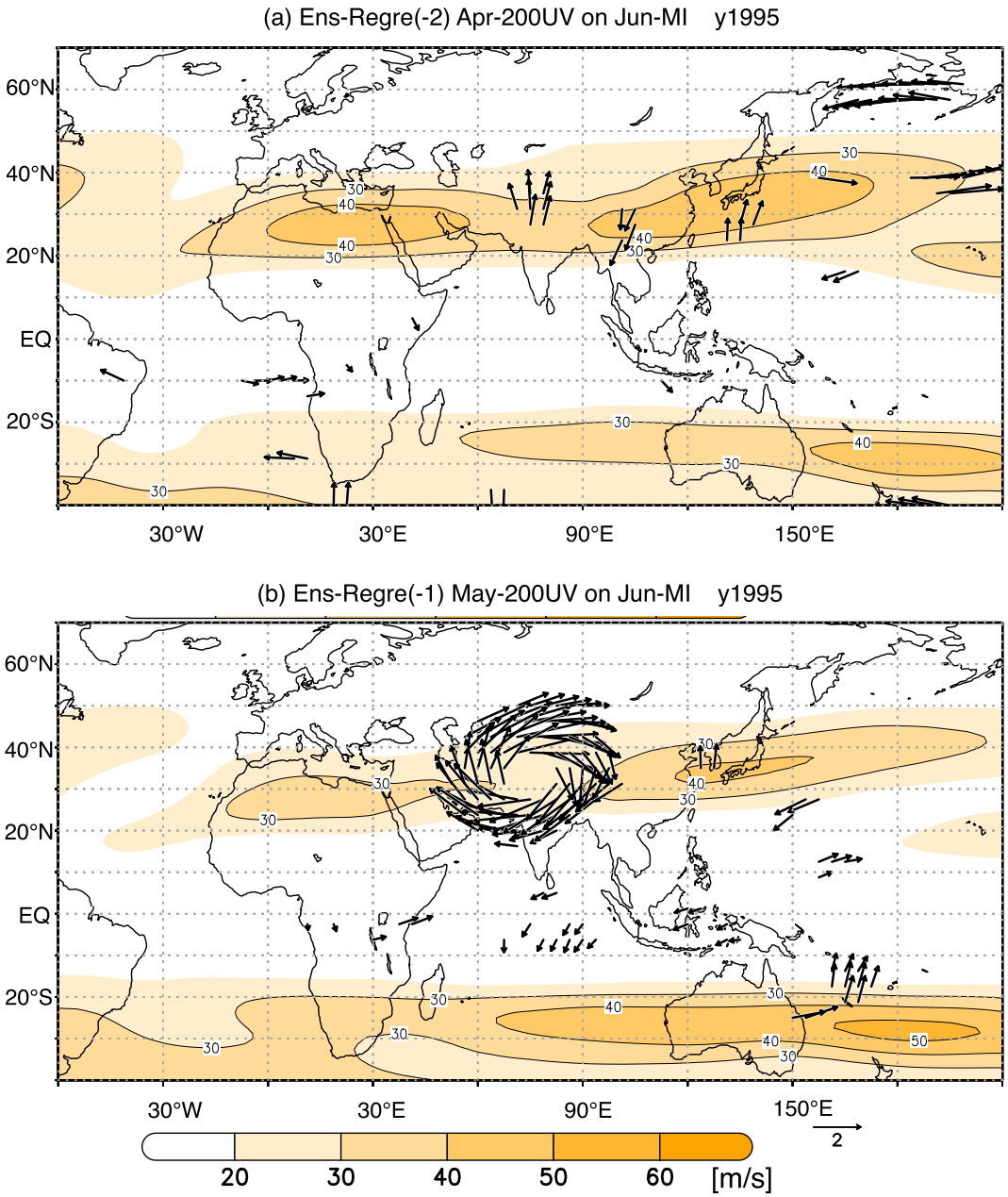

Fig. 4 **a** Lag-inter-ensemble regression map of April 200-hPa circulations on June MI in 1995. **b** Lag-inter-ensemble regression map of May 200-hPa winds on June MI. All plotted regressions were statistically significant inter-ensemble correlations at $p < 0.01$ (two-tailed Student's t test). Colors show the ensemble mean 200-hPa zonal wind speed to represent the Asian jet stream

The results show that the May-SAT impacts on June MI can be sufficiently extracted from internal climate variability. However, the impacts of winter and early spring land-surface conditions on the summer monsoon was small. We also examine how upper-tropospheric circulations affect SAT_{TP} (Fig. 4). In May, conspicuous anti-cyclonic signals are found over and around the Tibetan Plateau at the 200-hPa level, which is physically consistent with SAT_{TP} warming. An anti-cyclonic signal is found along the Asian subtropical jet stream, although no Rossby-wave propagation signals are identified. When backtracking in time, significant anti-cyclonic signals can only be detected in May, but not in April. Thus, the SAT_{TP} warming (cooling) is mainly associated with upper-level anti-cyclonic (cyclonic) anomalies in May from the case of 1995.

3.2.2 Interannual variability of land–atmosphere coupling activity over Asia and possible linkages to tropical SST anomalies

We now extend the analysis of the impacts of land-surface conditions to other years under different background SST conditions. More cases are selected based on ENSO phases because the ENSO-related SST anomalies affect the Asian monsoon.

Figure 5 includes the inter-ensemble correlation between June MI and May SATs in the developing El Ni$\tilde{n}$o (EL) years of 1997 and 2002, developing La Ni$\tilde{n}$a (LA) years of 2007 and 1984, the post (decaying) El Ni$\tilde{n}$o (post-EL) years of 2010 and 1998, and post (decaying) La Ni$\tilde{n}$a (post-LA) years of 2008 and 1985. The *active L–A year* and *inactive L–A year* cases are subjectively sampled for each ENSO phase because all the four ENSO phase years include almost evenly both *active L–A* and *inactive L–A* years. The strength of the *active L–A* signals is quantified in Sect. 3.3.

In 1997, 2007, 2010, and 2008 (Fig. 5), significant positive signals over and around the Tibetan Plateau imply that warmer May SAT over the Tibetan Plateau is associated with stronger June MI (as shown in Figs. 3 and 5). Negative SAT signals are sometimes observed over the southern parts of South and Southeast Asia (e.g., 2008, 1997, and 2010). Both indicate an enhanced large-scale north–south SAT gradient. Consequently, warmer SATs over the Tibetan Plateau and cooler pre-June SATs over South and Southeast Asia intensify June MI more than in normal years.

The inter-ensemble correlations between June MI and May 850-hPa circulation and precipitation are shown in Fig. 6. In the lower troposphere, enhanced cyclonic signals with increased precipitation over and around the Bay of Bengal are clearly found in 1997 and 2008. However, similar cyclonic signals are weaker in 2007 and 2010. Thus, the enhancement of May low-level winds and precipitation signals can not always enhance June MI. Although the low-level circulation and precipitation signals are limited, the enhanced low-level cyclonic circulation with precipitation activity can be understood as the early onset of the Asian monsoon or tropical cyclones over the Bay of Bengal through the adiabatic heating effects of precipitation on the development of the South Asian high. Climatologically, tropical cyclones over the North Indian Ocean frequently develop in the boreal spring and fall (e.g., Takahashi 2011).

Fig. 5 Lag-inter-ensemble correlation map between June MI and May SAT in **a** 1997, **b** 2007, **c** 2010, **d** 2008, **e** 2002, **f** 1984, **g** 1998, and **h** 1996, to represent the MI-related spatial pattern of SAT. Both years in the first row (**a, e**) are EL years, the second row (**b, f**) represents LA years, the third row (**c, g**) contains port-EL years, and the bottom row (**d, h**) depicts post-LA years, respectively. Panels in the left and right columns are *active* and *inactive L–A* years, respectively, selected subjectively in a manner consistent with the objective results in Sect. 3.3 (Fig. 10). All plotted correlations were statistically significant at $p < 0.01$ (two-tailed Student's t test)

The 200-hPa circulation is also shown in Fig. 7. Enhanced anti-cyclonic circulations over and around the Tibetan Plateau are found in the upper troposphere. Upper-level anti-cyclonic signals are found mostly in years with significant SAT signals (Figs. 5a–d and 7a–d). In contrast, the upper-level wind signals are also unclear in years with less clear SAT signals (Fig. 7e–h). Thus, the results of May 200-hPa winds associated with June MI can be consistent with those of May SATs associated with June MI. Because the 200-hPa signals are more systematic than those of the 850-hPa winds, the upper-level circulations in May significantly contribute to the inter-ensemble variations of the L–A interactions.

Also, the inter-ensemble regression of the May 200-hPa winds onto the May SAT_{TP} support that anomalous anti-cyclonic (cyclonic) circulation is associated with warmer (colder) SAT_{TP} (Fig. 8). All inter-ensemble regression maps show clear anti-cyclonic signals over and around the Tibetan Plateau. In addition, two other anti-cyclonic signals were often found in the upstream and downstream regions of the Sahara Desert and East Asia along the Asian jet stream. This result indicates that SAT_{TP} is warmer when anomalous anti-cyclonic circulation occurs around the Tibetan Plateau.

To understand how upper-level anti-cyclonic (cyclonic) signals are associated with land-surface warming (cooling), inter-ensemble correlations between June MI and shortwave radiation heating at the surface in May are examined for each year. Here, the net shortwave radiation at the surface (downward shortwave radiation - upward shortwave radiation) is used. Based on the subjective selection of the analyzed years, clearer signals are observed in 1997, 2007, 2010,

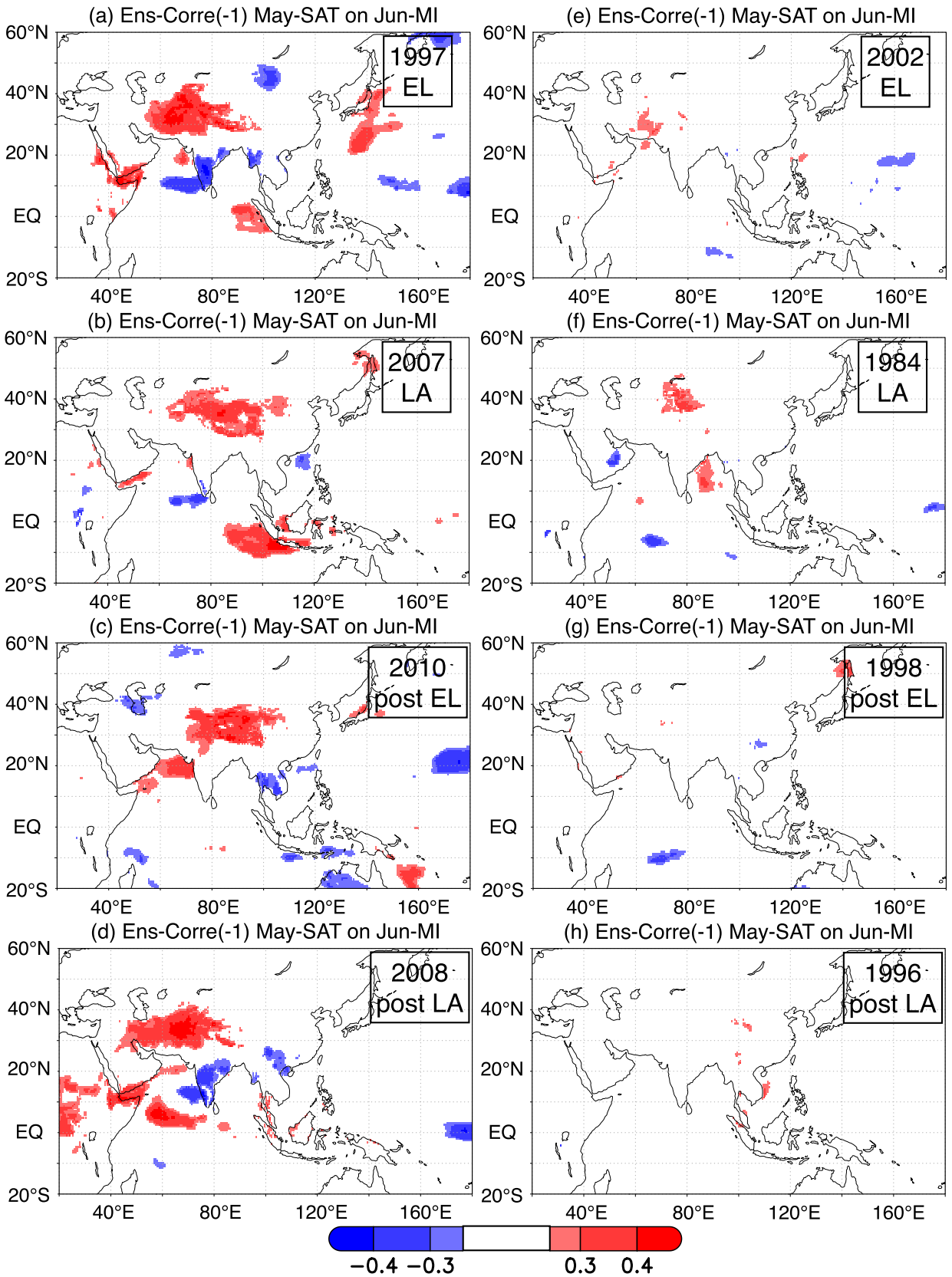
(a) Ens-Corre(-1) May-SAT on Jun-MI
1997
EL
(e) Ens-Corre(-1) May-SAT on Jun-MI
2002
EL
(b) Ens-Corre(-1) May-SAT on Jun-MI
2007
LA
(f) Ens-Corre(-1) May-SAT on Jun-MI
1984
LA
(c) Ens-Corre(-1) May-SAT on Jun-MI
2010
post EL
(g) Ens-Corre(-1) May-SAT on Jun-MI
1998
post EL
(d) Ens-Corre(-1) May-SAT on Jun-MI
2008
post LA
(h) Ens-Corre(-1) May-SAT on Jun-MI
1996
post LA
60°N
40°N
20°N
EQ
20°S
40°E
80°E
120°E
160°E
−0.4 −0.3
0.3 0.4

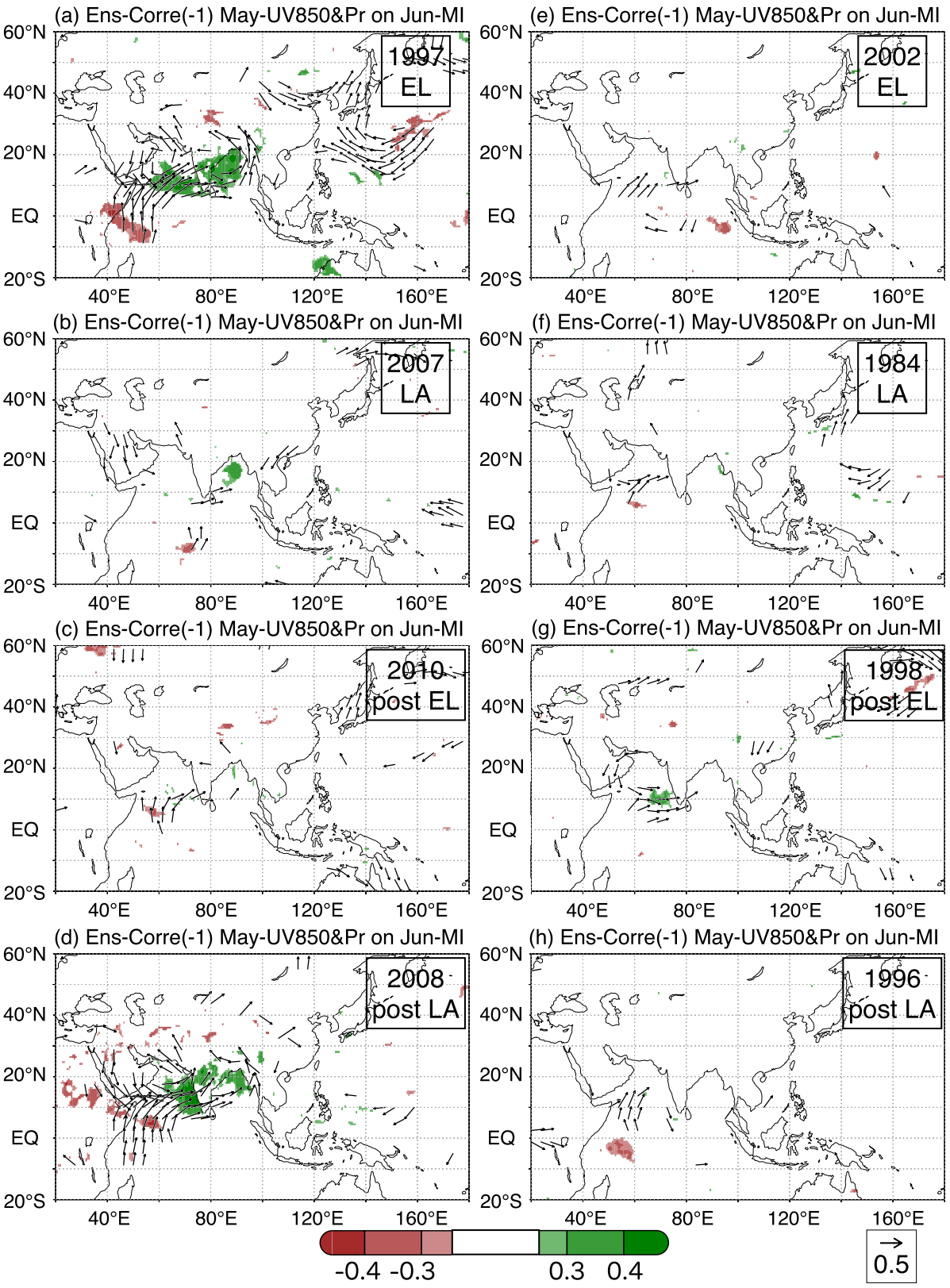
(a) Ens-Corre(-1) May-UV850&Pr on Jun-MI
1997
EL
(e) Ens-Corre(-1) May-UV850&Pr on Jun-MI
2002
EL
(b) Ens-Corre(-1) May-UV850&Pr on Jun-MI
2007
LA
(f) Ens-Corre(-1) May-UV850&Pr on Jun-MI
1984
LA
(c) Ens-Corre(-1) May-UV850&Pr on Jun-MI
2010
post EL
(g) Ens-Corre(-1) May-UV850&Pr on Jun-MI
1998
post EL
(d) Ens-Corre(-1) May-UV850&Pr on Jun-MI
2008
post LA
(h) Ens-Corre(-1) May-UV850&Pr on Jun-MI
1996
post LA
60°N
40°N
20°N
EQ
20°S
40°E
80°E
120°E
160°E
-0.4 -0.3
0.3 0.4
0.5

◂**Fig. 6** Lag-inter-ensemble correlation map between June MI and May 850-hPa winds (vectors) and precipitation (colors) in **a** 1997, **b** 2007, **c** 2010, **d** 2008, **e** 2002, **f** 1984, **g** 1998, and **h** 1996, to represent the MI-related spatial pattern of 850-hPa winds and precipitation. Both years in the first row (**a, e**) are EL years, the second row (**b, f**) represents LA years, the third row (**c, g**) contains port-EL years, and the bottom row (**d, h**) depicts post-LA years, respectively. Panels in the left and right columns are *active* and *inactive L–A* years, respectively, selected subjectively in a manner consistent with the objective results in Sect. 3.3 (Fig. 10). All plotted correlations were statistically significant at $p < 0.01$ (two-tailed Student's t test)

and 2008 (Fig. 9a–d) than in 2002, 1984, 1998, and 1996 (Fig. 9e–h), although the signals are less clear than with SAT. Additionally, the inter-ensemble correlations between June MI and May cloud cover are analyzed (not shown). The results are very similar to those of the net shortwave radiation (Fig. 9). Overall, during years with strong coupling between MI and SAT over and around the Tibetan Plateau, anti-cyclonic (cyclonic) anomalies were associated with less (more) cloud cover in May. The less cloud cover likely results in more shortwave radiation heating at the surface (Fig. 9).

Concurrent with the strong MI in June, the Tibetan Plateau and surrounding areas experience physically consistent signals of warmer SATs, upper-level anti-cyclonic development, increased net shortwave radiation, and decreased cloud cover. Thus, the inter-ensemble signals are physically consistent signals, and not statistically apparent relationships. In d4PDF, land-surface conditions on the Tibetan Plateau in late spring are likely to influence the Asian monsoon circulation in early summer, but the influence varies from year to year.

The relationship between June MI and May SAT over and around the Tibetan Plateau varies interannually, which may be associated with interannual variations of SST conditions. However, as previously mentioned, EL and post-EL years include both *active* and *inactive L–A* years, respectively. This implies that major climate variability indices of ENSO and Indian Ocean Dipole (IOD) can not simply explain the conditions of *active* and *inactive L–A* years. We attempt to understand the relationship between SST conditions and *active* and *inactive L–A* years in Sect. 3.4. Before that, Sect. 3.3 defines quantifying the L–A relationship of the Asian summer monsoon.

3.3 Interannual variations of land–atmosphere coupling activity

To quantify the impact of land-surface conditions on the Asian monsoon circulation for each year, we define a key area of land-surface impact based on the findings from Sect. 3.2. Because May SAT signals, which are correlated to June MI, roughly correspond to the Tibetan Plateau and its west, the key region here extends across 28°N–40°N, 60°E–100°E, which includes parts of South Asia, such as Afghanistan, Pakistan, and India. The SAT averaged over the key region, SAT_{TP}, has been defined in Sect. 2.2.

As mentioned, because May SAT_{TP} are physically associated with the Asian monsoon circulation in June, the strength of the SAT_{TP} signals should be closely associated with land–atmosphere coupling processes under the same SSTs. The normalized area (area-weighted number of grid points) of the statistically significant inter-ensemble correlation is calculated at the 99%-level between June MI and May SATs for each year (Fig. 10), which likely represents the strength of the L–A relationship. For example, high-value years correspond to clear signal years (e.g., 1997, 2007, 2010, 2008). The normalized area values are low in 2002, 1984, 1998, and 1996. Overall, the normalized area of the statistically significant inter-ensemble correlation between June MI and May SATs can represent the L–A coupling strength over Asia, which is referred to as the active *L–A index* in this study.

Furthermore, the active *L–A index* may be simply explained by ENSO phases because ENSO is the major atmosphere-ocean mode on in the Earth climate system. Unlike we expected, no significant relationship was revealed between the *L–A index* and SST anomalies over the equatorial central Pacific (e.g., the Ni$\tilde{n}$o 3 region) in either spring or summer. Actually, the correlation coefficients between active *L–A index* and Ni$\tilde{n}$o 3 SST in April, May, and June are 0.19, 0.15, and 0.25 ($p = 0.28$, $p = 0.44$, and $p = 0.17$), respectively. This result implies that these equatorial SST anomalies in these seasons cannot simply explain the L–A coupling activity over Asia. Notably, this result is consistent with the fact that both *active and inactive L–A* years are almost evenly included in the four ENSO phases.

3.4 What determines the interannual variability?

The inter-ensemble relationship between the Asian monsoon circulation and land-surface conditions, namely the L–A coupling process, which was quantified as the *L–A index* above, varies interannually. One idea to understand why the L–A coupling processes are only sometimes noticeable is that SST forcing is generally stronger than land-surface forcing. The key to this may be that the land-surface forcing becomes noticeable when stronger ocean-related forcing is weakened.

As mentioned in Sects. 3.2 and 3.3, dominant SST forcings such as ENSO and IOD cannot explain the time series of the *L–A index*. In addition, SST forcing can control the

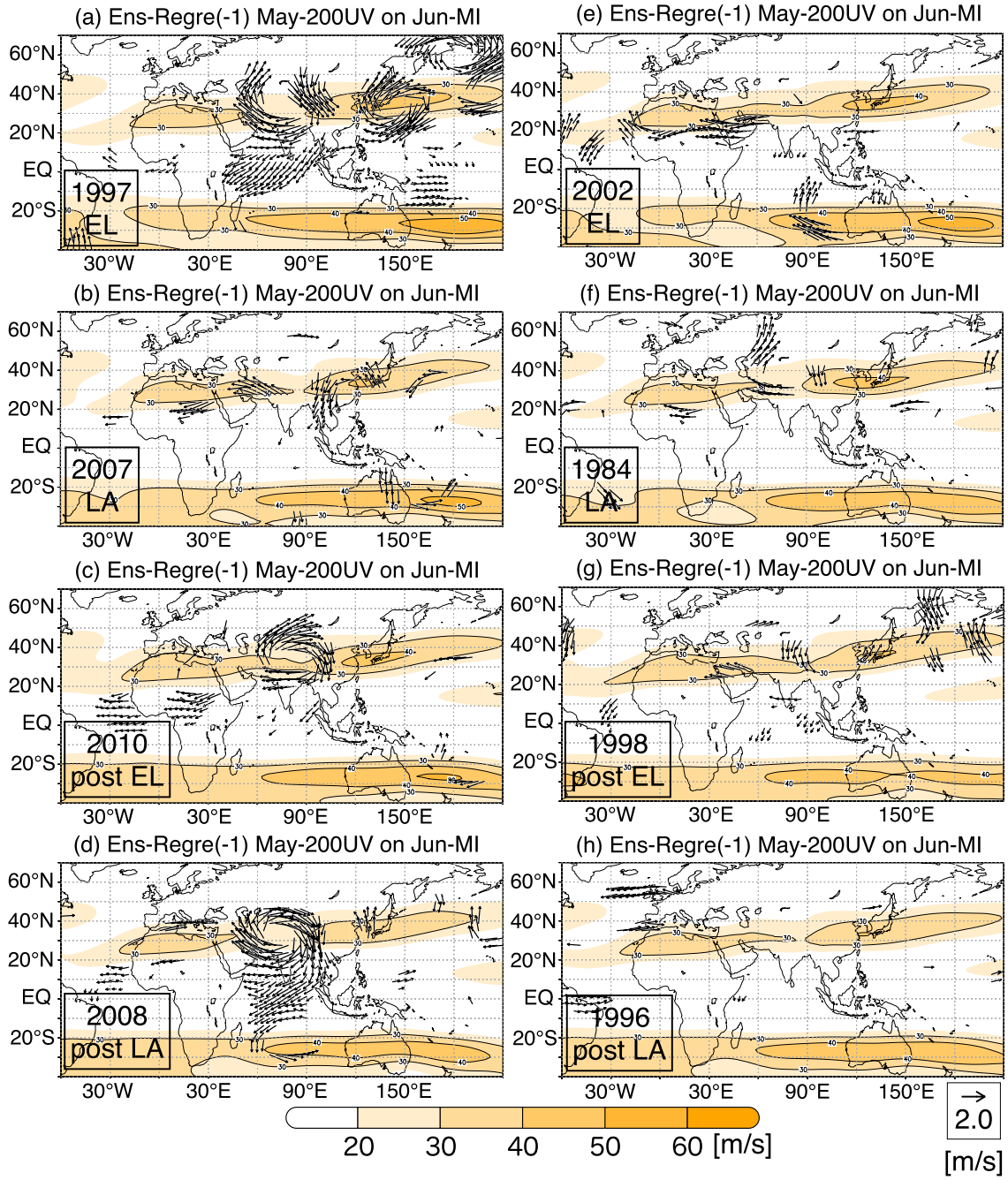

Fig. 7 Lag-inter-ensemble regression map of May 200-hPa winds on June MI in **a** 1997, **b** 2007, **c** 2010, **d** 2008, **e** 2002, **f** 1984, **g** 1998, and **h** 1996, to represent the MI-related spatial pattern of 200-hPa winds. Both years in the first row (**a, e**) are EL years, the second row (**b, f**) represents LA years, the third row (**c, g**) contains port-EL years, and the bottom row (**d, h**) depicts post-LA years, respectively. Panels in the left and right columns are *active* and *inactive L–A* years, respectively, selected subjectively in a manner consistent with the objective results in Sect. 3.3 (Fig. 10). All plotted regressions were statistically significant inter-ensemble correlations at $p < 0.01$ (two-tailed Student's t test). Colors show the ensemble mean 200-hPa zonal wind to represent the position of the Asian jet stream

ensemble-mean MI and SAT; for example, an SST forcing of a year induces a mean warm SAT condition; the warm SAT condition melts snow earlier, which in turn can affect L–A variability. However, the correlation coefficients between the *L–A index* and the medians of MI (Fig. 1) and SAT_{TP} (Fig. 2) are also close to zero. Thus, these possible processes do not explain the L–A variation.

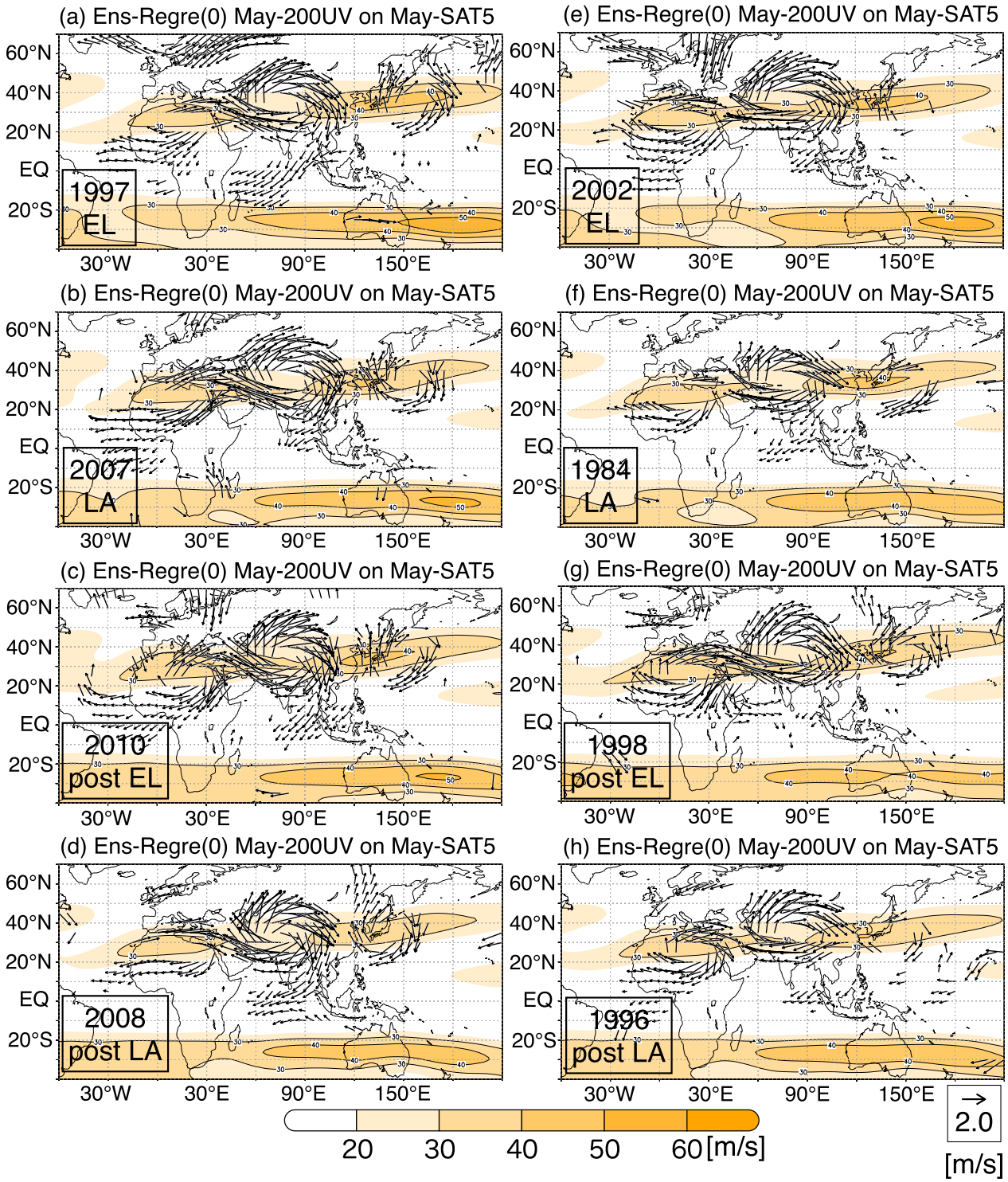

Fig. 8 Simultaneous inter-ensemble regression map of May 200-hPa winds on the May SAT_{TP} in **a** 1997, **b** 2007, **c** 2010, **d** 2008, **e** 2002, **f** 1984, **g** 1998, and **h** 1996, to represent the SAT_{TP}-related spatial pattern of 200-hPa winds. Note that the index used for the regression and correlation in this figure differed from Figs. 5, 6, 7. Both years in the first row (**a, e**) are EL years, the second row (**b, f**) represents LA years, the third row (**c, g**) contains port-EL years, and the bottom row (**d, h**) depicts post-LA years, respectively. Panels in the left and right columns are *active* and *inactive L–A* years, respectively, selected subjectively in a manner consistent with the objective results in Sect. 3.3 (Fig. 10). All plotted regressions were statistically significant inter-ensemble correlation at $p < 0.01$ (two-tailed Student's t test). Colors show the ensemble mean 200-hPa zonal wind to represent the position of the Asian jet stream

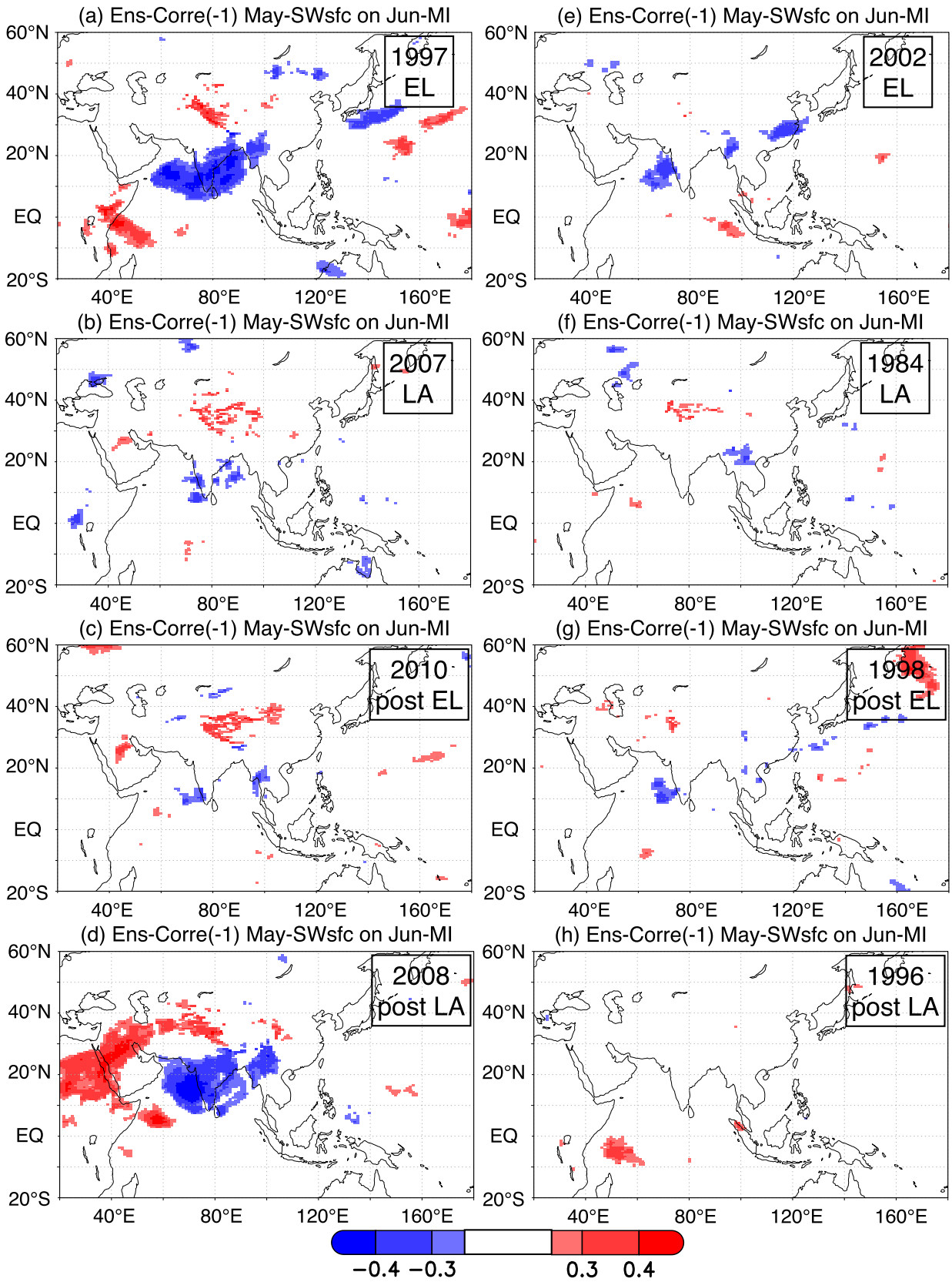
(a) Ens-Corre(-1) May-SWsfc on Jun-MI
1997
EL
(e) Ens-Corre(-1) May-SWsfc on Jun-MI
2002
EL
(b) Ens-Corre(-1) May-SWsfc on Jun-MI
2007
LA
(f) Ens-Corre(-1) May-SWsfc on Jun-MI
1984
LA
(c) Ens-Corre(-1) May-SWsfc on Jun-MI
2010
post EL
(g) Ens-Corre(-1) May-SWsfc on Jun-MI
1998
post EL
(d) Ens-Corre(-1) May-SWsfc on Jun-MI
2008
post LA
(h) Ens-Corre(-1) May-SWsfc on Jun-MI
1996
post LA
60°N
40°N
20°N
EQ
20°S
40°E
80°E
120°E
160°E
−0.4 −0.3
0.3 0.4

◂**Fig. 9** Lag-inter-ensemble correlation map between June MI and May net shortwave radiation (downward shortwave radiation - upward shortwave radiation) at the surface in **a** 1997, **b** 2007, **c** 2010, **d** 2008, **e** 2002, **f** 1984, **g** 1998, and **h** 1996, to represent the MI-related spatial pattern of SAT. Both years in the first row (**a, e**) are EL years, the second row (**b, f**) represents LA years, the third row (**c, g**) contains port-EL years, and the bottom row (**d, h**) depicts post-LA years, respectively. Panels in the left and right columns are *active* and *inactive L–A* years, respectively, selected subjectively in a manner consistent with the objective results in Sect. 3.3 (Fig. 10). All plotted correlations were statistically significant at $p < 0.01$ (two-tailed Student's *t* test)

To investigate the SST pattern related to the *L–A index*, a correlation analysis is performed between the prescribed SST averaged from April to May of the same year and the *L–A index*. The results reveal a negative correlation in the southern ocean of the Maritime continent and in surrounding Australia (Fig. 11). This indicates that when SSTs in the southern ocean of the Maritime continent and in surrounding Australia are cooler than normal, the influence of land-surface conditions on MI can be dominant. In contrast, warmer SST anomalies over the oceanic region suppress the role of land-surface conditions in monsoon circulation.

To understand the possible processes from the cooler SSTs around the southern Maritime continent to the monsoon circulation, we show the ensemble-mean 850-hPa zonal wind anomalies $\bar{u}_{ens}$ in May from the interannual and inter-ensemble means, which are normalized by the inter-ensemble standard deviations of the 850-hPa zonal wind $\sigma_{u-inter-ensemble}$ (Figs. 12 and 13). The normalized anomalies $\bar{u}_{ens}/\sigma_{u-inter-ensemble}$ for each year provide a measure of the signal-to-noise ratio.

Concurrent with the cooler SSTs in the *active L–A* years, divergence signals in the lower troposphere are clearly observed in May in six out of the seven years, except in 2010 (Fig. 12). The divergence signals over the Maritime continent are almost associated with easterly anomalies in the equatorial Indian Ocean and westerly anomalies in the western equatorial Pacific. However, in 2007, westerly anomalies over the equatorial Pacific are weak. In addition, the upper-level zonal wind signals show enhanced convergence over the Maritime continent (not shown). Over the Asian monsoon region, weakening of the Walker circulation over the equatorial and northern Indian Ocean and undeveloped monsoon circulation are found in the *active L–A* years. In contrast, a strengthening of the Walker circulation or earlier development of the monsoon circulation are often found in the *inactive L–A* years (Fig. 13).

In May of the developing stage of the Asian monsoon, the weaker Walker circulation or undeveloped monsoon circulation is favorable for the development of the Asian monsoon circulation by the L–A coupling process. Under these conditions, the role of the L–A coupling can be more visible. The

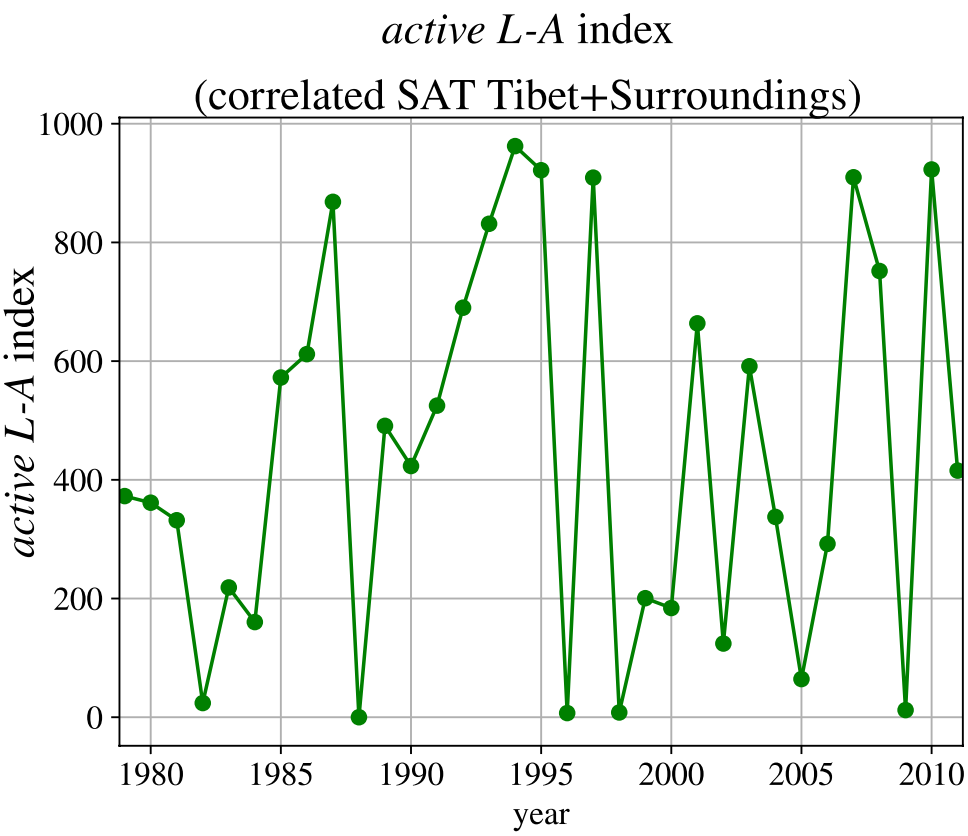

Fig. 10 The time-series of the *active L–A index* derived from the area of statistically significant inter-ensemble correlation between MI in June and SAT in May for each year. Target area roughly corresponded to the Tibetan Plateau and its surroundings (28°N–40°N, 60°E–100°E), as determined based on the results of the inter-ensemble correlation in Sect. 3.2. The *active L–A index* likely represents the coupling strength between June MI and May SATs over the key region

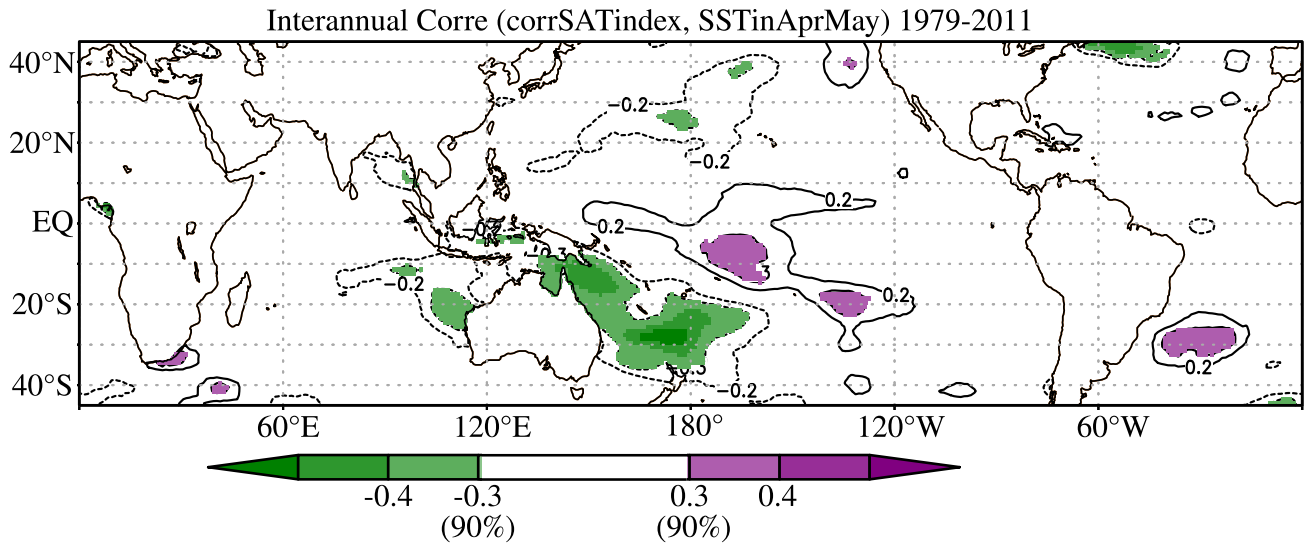

Fig. 11 *Interannual* correlation map between the *active L–A index* (Fig. 10) and SST anomalies averaged for April and May from 1979 to 2011. Positive values showed that SSTs show positive anomalies when the *active L–A index* was high. Color indicates the $p < 0.10$ significance limit of the *interannual* correlations, as determined by the Student's t test (degree of freedom is 31). Contours were plotted to represent the spatial pattern of *interannual* correlation. Note that this figure shows interannual correlation, not inter-ensemble

importance of the L–A coupling for the development of the Asian monsoon can be explained mainly by our hypothesis of whether the SST forcing is weaker than the internal climate variability or not, although this speculation may not be suitable for a small number of cases.

The weak Walker circulation over the equatorial and northern Indian Ocean with the cool SST anomalies over and around the southern ocean of the Maritime continent does not simply lead to a strong or weaker June MI. Rather, these conditions of weak forcing for the development of Asian monsoon circulation can enhance the L–A coupling fluctuation in both positive and negative directions. During *active L–A* years, both stronger MI with warm SATs and weaker MI with cooler SATs occur more frequently among the 100 ensemble members, indicating that internal climate variability is notable. Thus, when the Walker circulation conditions and monsoon circulation are weaker in May with anomalously cooler SSTs around the southern Maritime continent, land-surface forcing over the Asian monsoon region may become noticeable. However, the mechanisms underlying the interannual variability of the *L–A index* needs further studies.

4 Discussion

4.1 Persistence of land-surface signals from March to May

This subsection examines how land-surface conditions can explain May SAT_{TP} using d4PDF. Anomalous land-surface conditions over and around the Tibetan Plateau in early spring can not directly explain the subsequent early summer MI. Considering the physical processes of land-surface condition impact on June monsoon, there are stepwise processes. Here, the land-surface signals are not easily maintain through stepwise processes, from winter or early spring land-surface conditions to May SAT_{TP}, and further to the June monsoon. Generally, it is difficult to track season-long land-surface signals from winter and spring to the subsequent summer. For example, Senan et al. (2016) examined similar signals from April to early summer using a 15-ensemble forecasting system, suggesting that the persistence of land-surface signals from winter or early spring was not easy.

To briefly confirm the persistent influence of land-surface conditions on May SAT_{TP}, the lag-inter-ensemble correlations between May SAT_{TP} and the surface temperature or snow cover in January–February, February–March, and March–April are shown in Fig. 14. As expected, SAT_{TP} persistent impact is detectable from March–April. Here, we quantitatively analyze the extent to which the March SAT_{TP} signal persists through May. As mentioned in Sect. 2.1, because SAT and surface temperature anomalies on the monthly time-scale are highly negatively correlated with snow cover, the following results based on surface temperature anomalies remains similar even if surface temperature is replaced with snow cover (partly not shown).

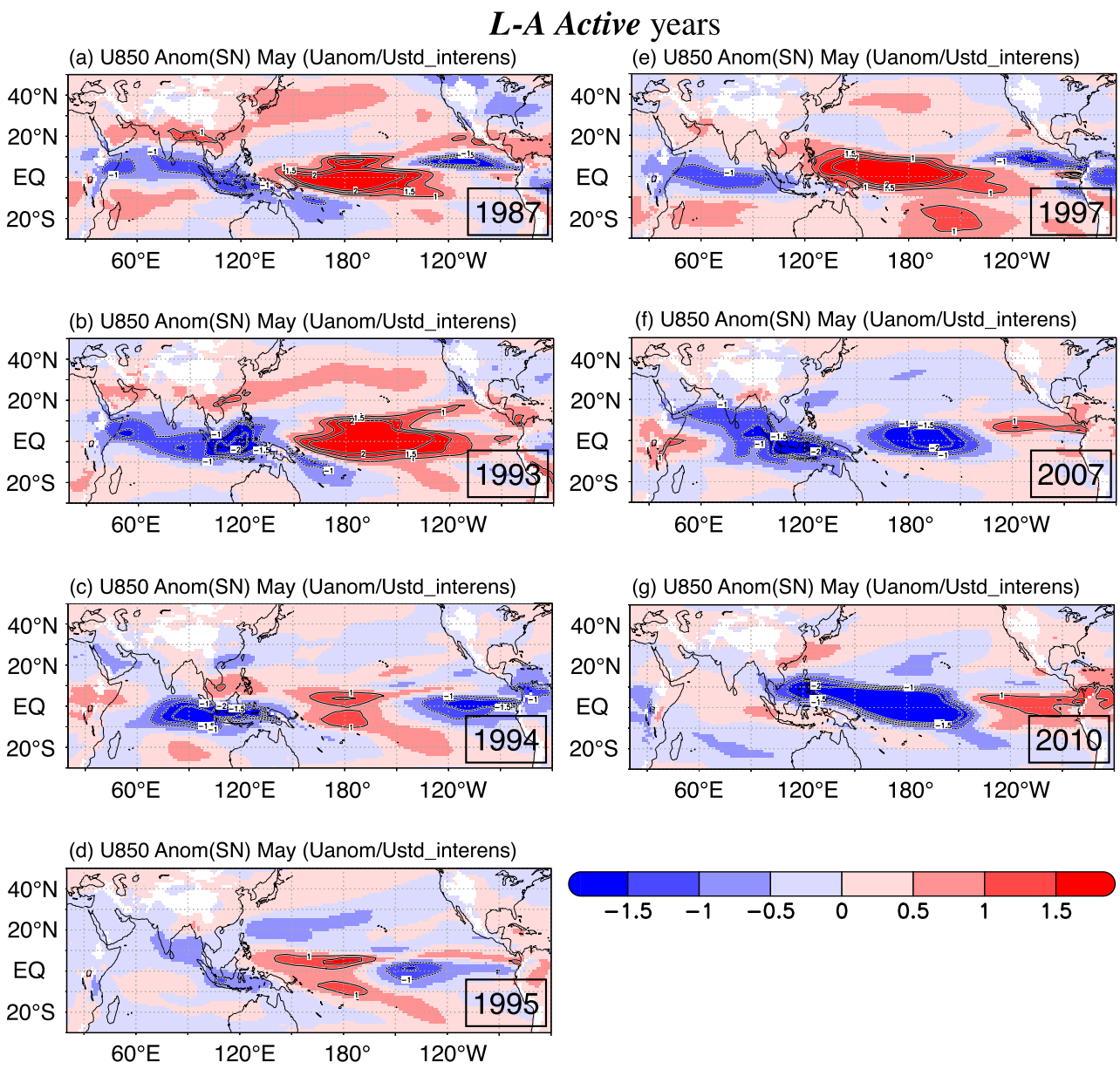

Fig. 12 Ensemble-mean 850-hPa zonal wind anomalies $\bar{u}_{ens}$ in May from the interannual and inter-ensemble means normalized by the inter-ensemble standard deviations of 850-hPa zonal wind $\sigma_{u-inter-ensemble}$ in *active L–A* years, **a** 1987, **b** 1993, **c** 1994, **d** 1995, **e** 1997, **f** 2007, and **g** 2010. The interannual and inter-ensemble means are all the averages of the 33 years and 100 ensembles (3300 samples). The normalized anomalies $\bar{u}_{ens}/\sigma_{u-inter-ensemble}$ indicate a measure of signal-to-noise ratio. Red (Blue) color indicates that the zonal wind anomalies are westerlies (easterlies)

4.1.1 Quantification from a lag-composite analysis

To quantify the impact of land-surface conditions, we use the inter-ensemble standard deviation of SAT_{TP} in May as a standard reference, $\widetilde{\sigma}_{SAT-sim}$, which is approximately 1.1 K (Fig. 15). Here, the square of this inter-ensemble standard deviation in the SAT_{TP} value is referred to as the total inter-ensemble variance in SAT_{TP}, which is used for comparison with the land-surface influence signals.

To determine the impact of early spring (March) land-surface conditions on late spring (May) SAT, we estimate the land-surface signal from the lag composite analysis by creating lag composite boxplots. First, a total of 50 members, the top 25% and bottom 25%, are selected based on the March surface temperature (not SAT) over the key region. Next, we use the lag composite method on the March, April, and May SAT_{TP} to track the March, April, and May SAT_{TP} statuses of the top 25% and bottom 25% groups (Fig. 16). The results

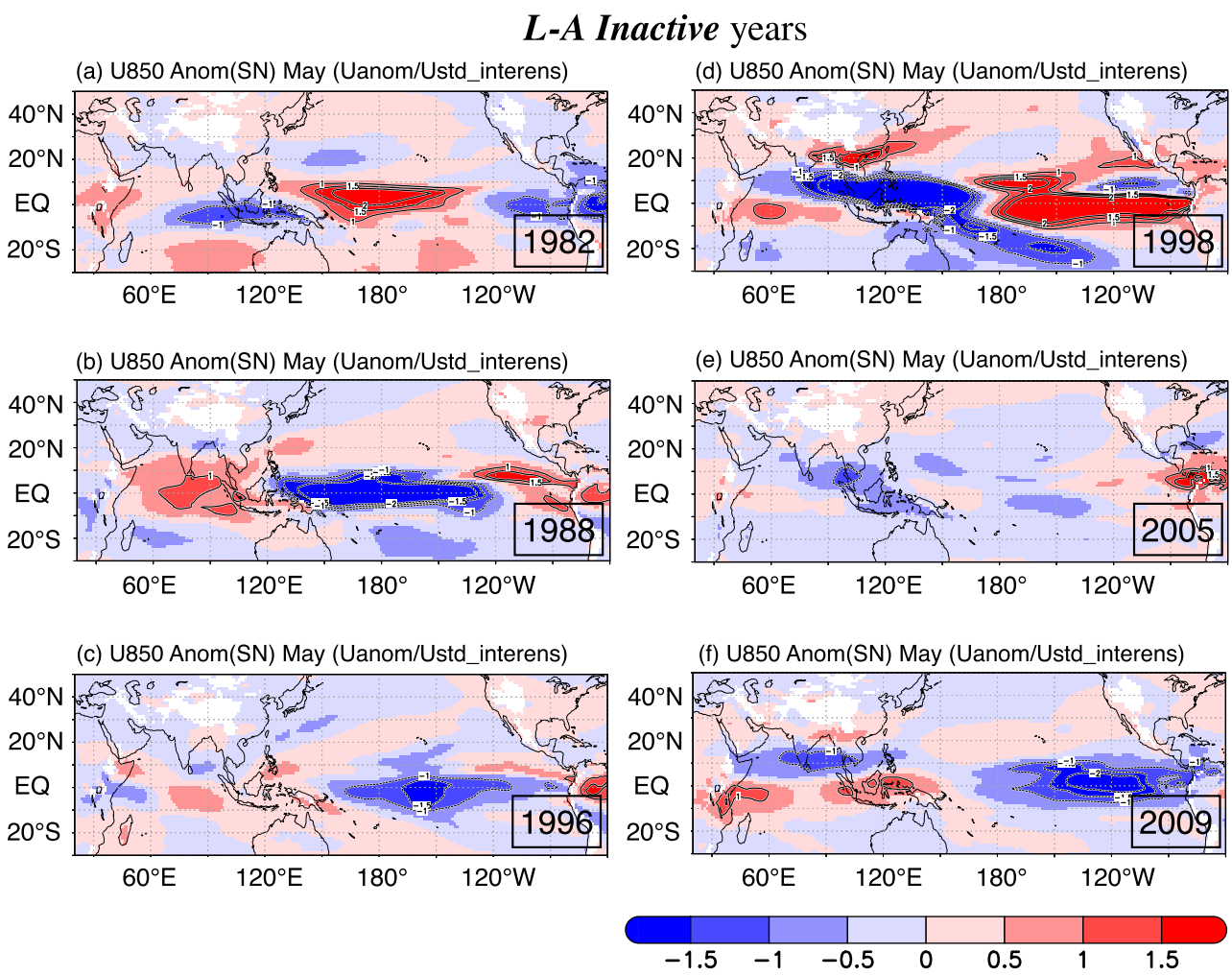

Fig. 13 Ensemble-mean 850-hPa wind anomalies $\bar{u}_{ens}$ from the inter-annual and inter-ensemble means normalized by the inter-ensemble standard deviations of 850-hPa wind $\sigma_{u-inter-ensemble}$ in *inactive L–A* years, **a** 1982, **b** 1988, **c** 1996, **d** 1998, **e** 2005, and **f** 2009. The normalized anomalies $\bar{u}_{ens}/\sigma_{u-inter-ensemble}$ indicate a measure of signal-noise-ratio. Red (Blue) color indicates that the zonal wind anomalies are westerlies (easterlies)

show that if the March land-surface signal persists significantly until May, the difference in SAT_{TP} between the two groups in May should be significant; if it does not persist, there should be no significant difference. The differences in the median of SAT_{TP} are tested for statistical significance at $p = 0.05$ with a median test (Mood's median test).

The results show that the difference in March SAT_{TP} was approximately 3–3.5 K, as estimated from the median values of each group (Figs. 16 and 17). Alternatively, the differences in May SAT_{TP}, as estimated from the median values of each group, range approximately from 0.5 to 0.7 K. As expected, the SAT_{TP} differences in May are smaller than those in March. These characteristics are similar across the eight sample years (Fig. 16). The statistically significant differences in the May SAT_{TP} medians between the two groups are occasionally found. Furthermore, the decrease in SAT_{TP} differences from March to May is explained by random atmospheric disturbances, although the inter-ensemble SAT_{TP} standard deviation in March is approximately 30% larger than that in May. The differences in the May medians between the top and bottom groups could be close to zero or small negative values in some years (Fig. 17), which could be associated with active atmospheric disturbances that mostly dampened the land-surface signals during spring. The same lag-composite analysis based on snow cover shows almost the same results, although the differences in March medians between the two groups based on snow cover are somewhat smaller than those based on surface temperature and statistically significant differences are found in some different years (Fig. 17).

Note that the years with the significant memory effects differ from the *active L–A* years because the memory effect

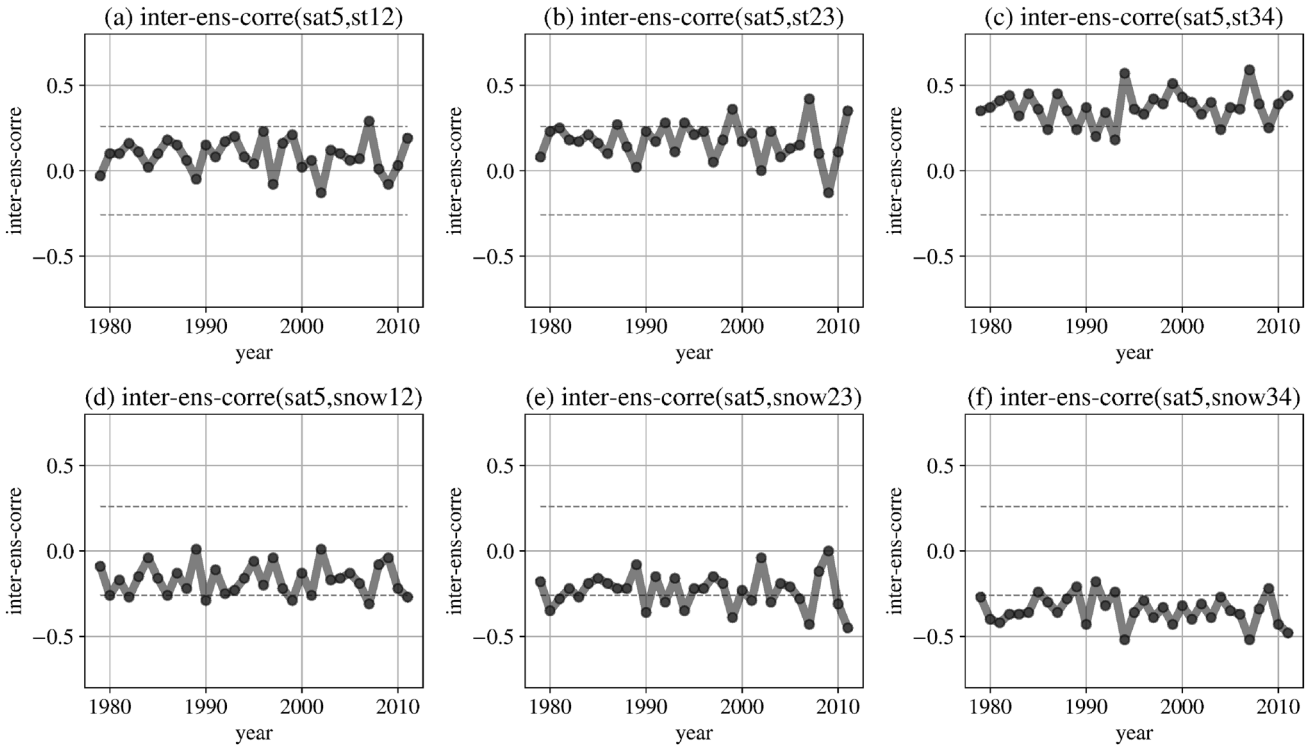

Fig. 14 The time-series of the inter-ensemble correlation between May SAT_{TP} and surface temperature averaged across **a** January–February, **b** February–March, and **c** March–April. **d**)–**f** are the same as (**a**–**c**) but for between May SAT_{TP} and snow cover. The surface temperature and snow cover were area-averaged over the key region (28° N–40°N, 60°E–100°E). Dashed lines indicate the $p < 0.01$ significance limit of the inter-ensemble correlations, as determined by the Student's *t* test

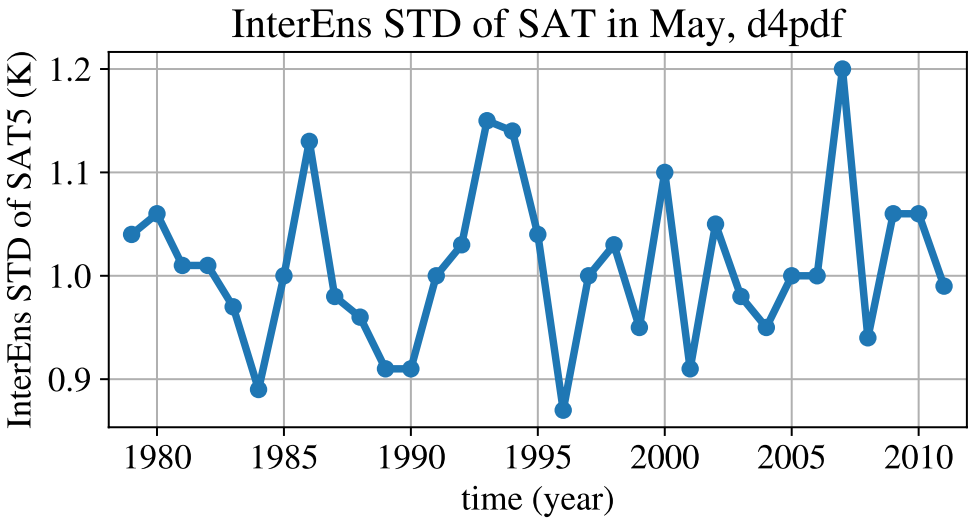

Fig. 15 The time-series of inter-ensemble standard deviations in the area-averaged May SAT_{TP} for each year

focuses on the spring period from March to May, whereas the *active L–A* is based on the relationship between June MI and May SAT. In addition, the years with the statistically significant median differences (Fig. 17) do not often correspond to the *active L–A* years (Fig. 10). These results suggest that early spring land-surface signals cannot easily influence June MI through the May SAT_{TP} signals, which is consistent with the results that the inter-ensemble correlation does not show statistically significant signals during the spring (Fig. 3).

Because the difference between the medians of the top 25% group and the bottom 25% group exceeds 0.6 K, the top

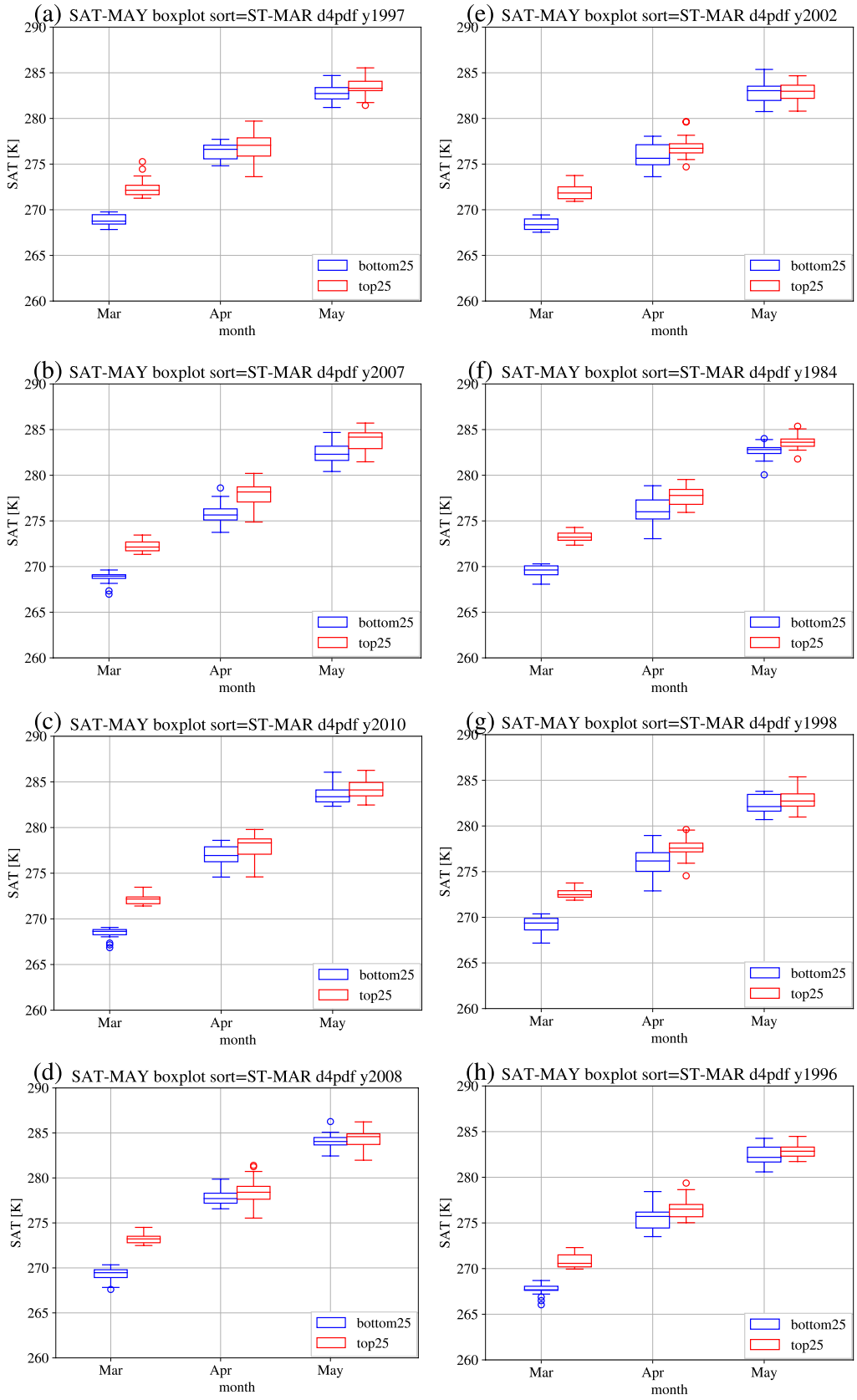
(a) SAT-MAY boxplot sort=ST-MAR d4pdf y1997
(e) SAT-MAY boxplot sort=ST-MAR d4pdf y2002
(b) SAT-MAY boxplot sort=ST-MAR d4pdf y2007
(f) SAT-MAY boxplot sort=ST-MAR d4pdf y1984
(c) SAT-MAY boxplot sort=ST-MAR d4pdf y2010
(g) SAT-MAY boxplot sort=ST-MAR d4pdf y1998
(d) SAT-MAY boxplot sort=ST-MAR d4pdf y2008
(h) SAT-MAY boxplot sort=ST-MAR d4pdf y1996
SAT [K]
290
285
280
275
270
265
260
Mar
Apr
May
month
bottom25
top25

◂**Fig. 16** Boxplot of SAT_{TP} in March, April, and May, which was lag-composite analysis, to represent the persistence of SAT_{TP} signals from March to May. Two categories were defined as the top and bottom 25% of March surface temperature over the key region among the 100 members. Blue (Red) boxplots indicate bottom (top) 25% samples based on March surface temperature over the key region. The years shown in this figure are the same as in Figs. 5, 6, 7, 8, 9

12.5% and bottom 12.5% of the sample may be considered capable of maintaining a 0.6-K signal until May. Thus, the probability of exceeding the 0.6-K signal in May may be 25% for the entire sample (the sum of the outer 12.5% of the samples on both sides). Hence, there can be a 25% chance that the impact of the March land-surface conditions on the May SAT_{TP} is ≥ 0.6 K, and a probability of 75% chance that it is ≤ 0.6 K.

Finally, the land-surface signals estimated above are compared to the inter-ensemble range of May SAT_{TP}. Because the inter-ensemble standard deviation of May SAT_{TP}, $\widetilde{\sigma}_{SAT-sim}$, is approximately 1.1 K, the inter-ensemble range of SAT_{TP} may be given as $2\widetilde{\sigma}_{SAT-sim}$ of approximately 2.2 K (Fig. 2). Hence, the impact of March land-surface conditions on May SAT_{TP} (estimated to be 0.6 K) is estimated to be 20–30%

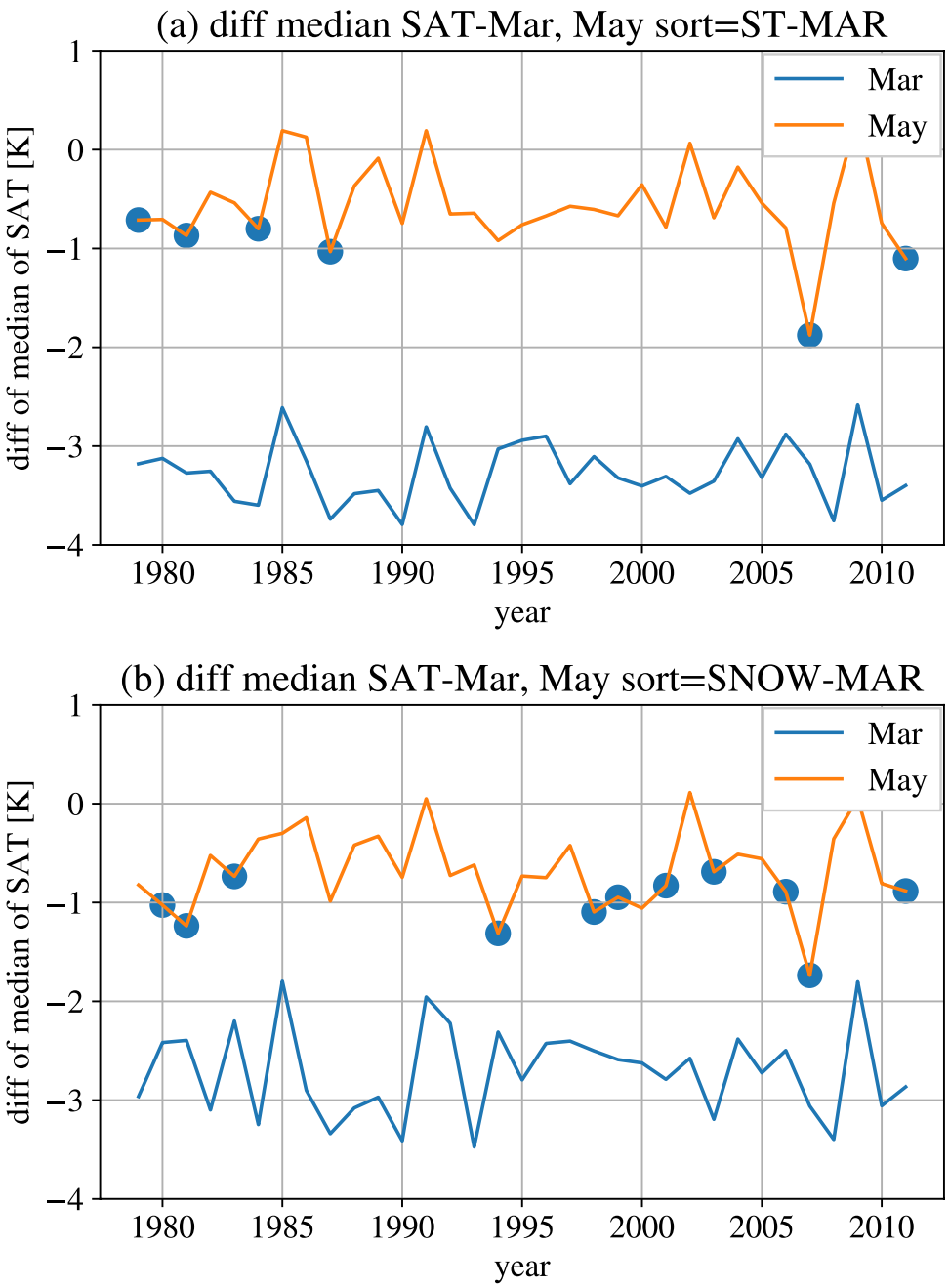

Fig. 17 Based on Fig. 16, **a** median SAT_{TP} differences between the two categories are shown for each year. **b** is the same as (**a**) but for the composite based on snow cover. The surface temperature and snow cover were area-averaged surface temperature over the key region when we determine the top and bottom 25% samples. Blue (Orange) solid line denotes the median SAT_{TP} differences in March (May). In the time series of May median SAT_{TP} differences, a blue circle indicates that the SAT_{TP} difference is statistically significant at $p = 0.05$ with a median test (Mood's median test)

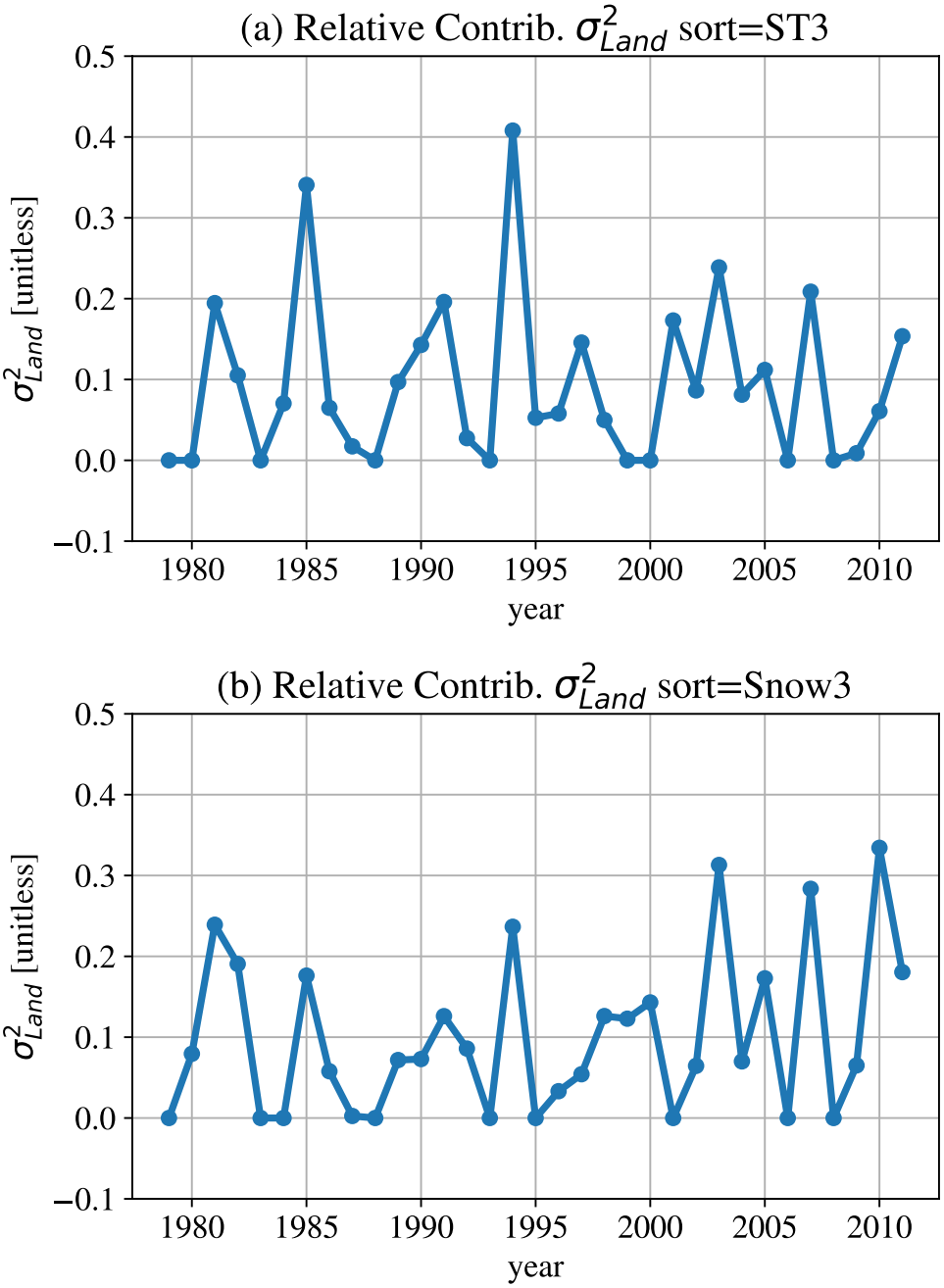

Fig. 18 **a** Time-series of σ^2_{Land} of May SAT_{TP}. σ^2_{Atmos} was calculated from 50 members that March surface temperature were close to the median of March surface temperature. Thus, initial land-surface conditions in March were similar among the 50 members. σ^2_{Tot} was calculated from all 100 members. Here, when σ^2_{Atmos} of May SAT_{TP} was $> \sigma^2_{Tot}$, σ^2_{Atmos} was assumed to equal σ^2_{Tot} (i.e., σ^2_{Land} is zero). **b** is the same as (**a**) except that the 50 members were selected based on snow cover

of the total inter-ensemble variability with a probability of 25%. Because the interannual variability associated with SST anomalies has a significant impact (Sect. 3.1), the estimated impact of land-surface conditions may be difficult to determine from the observed data.

4.1.2 Quantification from a variance analysis

In addition, the order of the impact of the March land-surface conditions on May SAT_{TP} is estimated using an analysis of variance. Because the AGCM experiment in a specific year is used for this calculation, the inter-ensemble variability consists of atmospheric and land-surface variabilities. Using only members with similar land-surface conditions in March, the inter-ensemble variance in May can be considered as atmospheric internal variability σ^2_{Atmos} (see later), which is the variance removed from the land-surface memory effects. This allows us to extract only the atmospheric internal variability. Specifically, all members, except for the top 25 and bottom 25 members (i.e., the 50 members closest to the median), are selected based on the March surface temperature (not SAT) over and around the Tibetan Plateau. The land-surface conditions of the selected

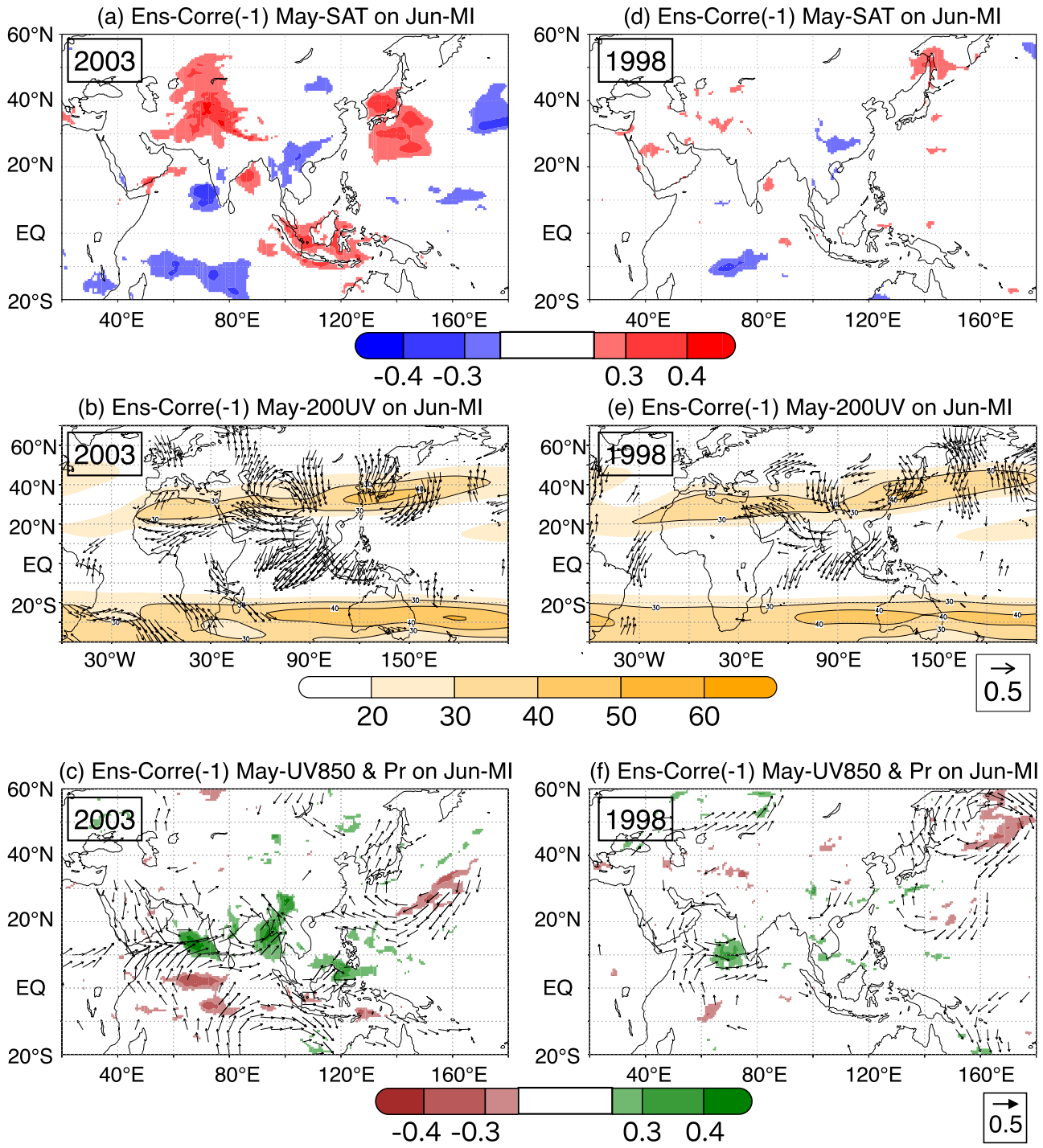

Fig. 19 Lag-inter-ensemble correlation map between June MI and (**a, d**) May SATs, (**b, e**) May 200-hPa circulations, and (**c, f**) May 850-hPa circulations (vectors) and precipitation (colors). Left panels (**a–c**) depict 2003, and right panels (**d–f**) show 1998. All plotted correlations were statistically significant at $p < 0.01$ (two-tailed Student's t test). Colors show the ensemble mean 200-hPa zonal wind speed to represent the Asian jet stream (**b, e**)

50 members are similar. Similar results are obtained when we use March snow cover instead of March surface temperature (not shown). Although similar land-surface conditions are selected in the key region, the land-surface conditions over the other regions may be different. Hence, land-surface influences outside the key region cannot be removed.

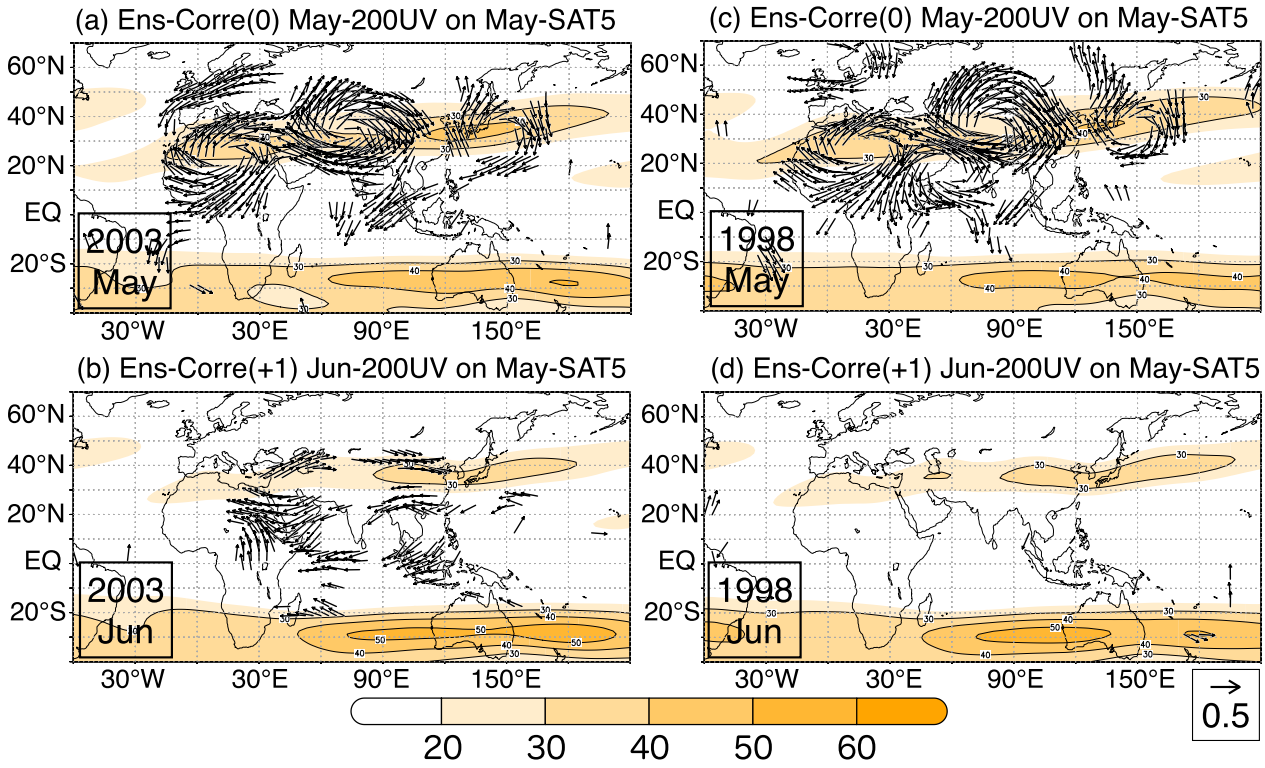

Fig. 20 **a, c** Simultaneous inter-ensemble correlation map between SAT_{TP} in May and upper-level (200 hPa) circulations in May. **b, d** Lag-inter-ensemble correlation map between the SAT_{TP} in May and June 200-hPa circulations, to represent May-SAT_{TP}-related upper-level circulation in June. Left panels (**a, b**) depict 2003, and right panels (**c, d**) show 1998. Note that the index used for the correlation calculation in this figure differed from Fig. 17. All plotted correlations were statistically significant at $p < 0.01$ (two-tailed Student's t test). Colors show the ensemble mean 200-hPa zonal wind speed to represent the Asian jet stream in May (**a, c**) and in June (**b, d**)

Two types of inter-ensemble SAT_{TP} variances are calculated in May. First, the total variance, σ^2_{Tot}, is the inter-ensemble and interannual variance of all members. Second, the variance without significant land-surface perturbations, σ^2_{Atmos}, is computed from the selected 50 ensemble members. The inter-ensemble variance explained by the March SAT_{TP} differences, σ^2_{Land} may be given by Eq. (2):

$$\sigma^2_{Land} = 1 - \sigma^2_{Atmos}/\sigma^2_{Tot} \tag{2}$$

where the second term on the right $\sigma^2_{Atmos}/\sigma^2_{Tot}$ takes a value between 0.0 and 1.0, but can potentially exceed 1.0 owing to differences in sample size and other random noise. When $\sigma^2_{Atmos} \geq \sigma^2_{Tot}$, it is assumed that σ^2_{Atmos} is equal to σ^2_{Tot}.

The results show that in average, 5%–20% of the variance in the May SAT_{TP} is contributed by land-surface conditions (Fig. 18a). When σ^2_{Land} is calculated based on March snow cover, we obtained similar estimations (Fig. 18b). Note that other LEns-AGCMs can be used to reduce uncertainty, albeit at a high computational cost.

It is noteworthy that similar contribution ratios are obtained from the different estimations, a lag-composite and variance analyses (Figs. 16, 18). Other estimates obtained via different experiments will be compared with the present AGCM or another LEns-AGCM in future research.

4.2 Predictability by land-surface conditions for the 2003 East Asian monsoon

This section discusses the land-surface influences in the past target years of 2003 and 1998, following Xue et al. (2021). Xue et al. (2021) proposed a scientific project to understand the impact of land-surface conditions, particularly over the Tibetan Plateau on the East Asian climate during late spring to early summer, focusing on 2003. Recent papers have shown that SAT anomalies over the Tibetan Plateau have downstream effects on the East Asian monsoon (e.g., Diallo et al. 2022). To further investigate another benchmark, a case of downstream impacts on East Asia is selected during a year of severe flooding in China (1998) because 1998 was also selected for comparison (e.g., Diallo et al. 2022).

In the present analysis, the 2003 patterns show marked SAT signals over and around the Tibetan Plateau associated

with June MI (Fig. 19a–c). Suppose that the May SAT over and around the Tibetan Plateau is hotter or cooler than the normal conditions. In this case, land-surface conditions may tend to influence the Asian monsoon climate and can contribute to subseasonal predictions over the Asian monsoon region.

On the other hand, the land-surface conditions may not have contributed to the East Asian summer monsoon of 1998 (Fig. 19). This weak signal is not surprising because post-EL forcing may have been significant in 1998 (Xie et al. 2009, 2016). The occurrence of severe flooding in China is less attributable to SST in 1998 because the ensemble-mean simulated precipitation for June and July do not show positive anomaly (not shown). Thus, the 1998 flood in China may have occurred largely by internal natural variability. Although this understanding may depend on the numerical model used, under the post-EL oceanic forcing in 1998, most ensemble members do not simulate major flooding or increased precipitation. Actually, observational studies (Wang et al. 2017) also suggest that the post-EL forcing on the East Asian climate is not always significant. It has also been suggested that the predictability of the post-EL is projected to decrease under a warming climate (Jiang et al. 2018).

Finally, the inter-ensemble correlation between the SAT_{TP} and the 200-hPa winds is examined. In both years, the 200-hPa anomalous anti-cyclonic (cyclonic) circulation around the Tibetan Plateau in May is simultaneously associated with the warmer (colder) May SAT_{TP}. However, the June 200-hPa circulation signals associated with the May SAT_{TP} are more marked in 2003 than in 1998 (Fig. 20). Thus, under the SST conditions in 2003, the *L–A signals* are more likely to emerge and persist compared to 1998.

5 Conclusions

The present study quantifies the influence of land-surface conditions over the Eurasian continent, namely the Tibetan Plateau and its surrounding regions, on Asian monsoon circulations using the LEns-AGCM, d4PDF. Although interannual variations in the Asian monsoon circulation strength (MI) are primarily influenced by ENSO-related SST anomalies, such background anomalies vary interannually. Accordingly, the relationships between land-surface conditions and the Asian monsoon are separately extracted for each year, primarily using inter-ensemble correlation analysis. This method is designed to isolate the effects of land-surface conditions from an SST-prescribed AGCM large-ensemble dataset. It exploits the advantages of LEns-AGCM over observational and other types of global climate simulation datasets.

The results show that above-normal May SATs over and around the Tibetan Plateau can enhance the Asian monsoon circulation in June. The physical mechanism is that the warmed Tibetan Plateau and its surrounding regions enhance the north–south gradient of air temperature, resulting in the enhancement of monsoon circulation. In the upper troposphere, when anti-cyclonic circulation anomalies are robustly simulated in May, the monsoon circulation is strong in June. This can be interpreted as enhanced anti-cyclonic circulation anomalies along the Asian jet or an earlier northward migration of the Asian jet regarding its seasonal march. The appearance of upper-level circulation signals can control the interannual variability in SATs over and around the Tibetan Plateau. Although low-level cyclonic circulation anomalies with positive precipitation anomalies of the South and Southeast Asian monsoons could sometimes enhance the north–south SAT gradient, if it is not often. The simulated inter-ensemble variability can be confirmed as a process of enhancing the Asian monsoon in observational datasets. However, the influences of land-surface memory effects from January to April on the June MI are not detectable.

The influence of land-surface conditions is found vary from year to year, as the existence of stronger *external* SST forcing may overshadow possible effects of land-surface conditions. Accordingly, even though the effects of land-surface conditions are always present, it becomes detectable and play a more crucial role when the external forcing is weak. Active L–A coupling years coincide with years of cooler SSTs with anomalous low-level divergence and upper-level convergence over and around the Maritime continent, implying that SST forcing is associated with the L–A coupling strength. Specifically, in May, during the developing phase of the summer monsoon circulation, the weaker Walker circulation or undeveloped monsoon circulation, which are associated with SST forcing, is favorable for the development of Asian monsoon circulation by the L–A coupling process. In contrast, strong Walker or earlier formed monsoon circulations, which are also forced by SST anomalies, can overshadow the influence of the L–A coupling. However, contrary to what was expected, major interannual climate variabilities, such as ENSO and IOD, do not clearly coincide with the *active* and *inactive L–A* years, which should be investigated more in future studies.

Lag-composite and variance analyses show that the March surface-temperature and snow-cover anomalies over the key region gradually decline by May. Specifically, the memory effects of March land-surface conditions on May SAT are estimated to be 10–20% of the total inter-ensemble variance. The estimated values are not small, considering that the SST-forced SAT_{TP} interannual variance is 18% of the total SAT_{TP} interannual variance, although they may be difficult to compare simply. Using the LEns-AGCM, we

first quantified the memory effects of the land-surface conditions of the Tibetan Plateau on Asian monsoon circulation without oceanic forcing. Finally, because *active L–A* years can differ depending on the target region, season, and phenomenon, the regional and seasonal characteristics of the land-surface condition effects should be investigated in future studies.

Acknowledgements This work was partly supported by JSPS KAKENHI Grant 19H01375, 20H02252, and 22H00037 and the Environment Research and Technology Development Fund (JPMEERF20192004, JPMEERF20222002) of the Environmental Restoration and Conservation Agency provided by the Ministry of Environment of Japan. The d4PDF and JRA-55 datasets are available from the DIAS data archive system (https://diasjp.net/en/).

Author contributions HGT conceptualized, analyzed the data, and wrote the main manuscript text. SS and TS discussed and modified the manuscript. All authors reviewed the manuscript.

Funding Open access funding provided by Tokyo Metropolitan University. JSPS KAKENHI Grant 19H01375, 20H02252, and 22H00037. Environment Research and Technology Development Fund (JPMEERF20192004, JPMEERF20222002) of the Environmental Restoration and Conservation Agency Provided by the Ministry of Environment of Japan.

Data availability The d4PDF and JRA-55 datasets are available from the DIAS data archive system (https://diasjp.net/en/).

Declarations

Conflict of interest The authors have no competing interests to disclose.

References

Ailikun B, Yasunari T (2001) ENSO and Asian summer monsoon: persistence and transitivity in the seasonal march. J Meteorol Soc Jpn Ser II 79(1):145–159

Bamzai AS, Shukla J (1999) Relation between Eurasian snow cover, snow depth, and the Indian summer monsoon: an observational study. J Clim 12(10):3117–3132

Boos WR, Kuang Z (2010) Dominant control of the South Asian monsoon by orographic insulation versus plateau heating. Nature 463(7278):218–222

Brodzik MJ, Armstrong R (2013) Northern Hemisphere EASE-Grid 2.0 Weekly Snow Cover and Sea Ice Extent, Version 4. https://doi.org/10.5067/P7O0HGJLYUQU

Chen Z, Zhou T, Chen X, Zhang W, Zhang L, Wu M, Zou L (2022) Observationally constrained projection of Afro-Asian monsoon precipitation. Nat Commun 13(1):2552

Diallo I, Xue Y, Chen Q, Ren X, Guo W (2022) Effects of spring Tibetan Plateau land temperature anomalies on early summer floods/droughts over the monsoon regions of South East Asia. Clim Dyn 1–23

Geen R, Bordoni S, Battisti DS, Hui K (2020) Monsoons, ITCZs, and the concept of the global monsoon. Rev Geophys 58(4):2020–000700

Goswami BN, Xavier PK (2005) ENSO control on the south Asian monsoon through the length of the rainy season. Geophys Res Lett 32 (18)

Hahn DG, Shukla J (1976) An apparent relationship between Eurasian snow cover and Indian monsoon rainfall. J Atmos Sci 33(12):2461–2462

Hill SA (2019) Theories for past and future monsoon rainfall changes. Curr Clim Change Rep 5:160–171

Ishii M, Shouji A, Sugimoto S, Matsumoto T (2005) Objective analyses of sea-surface temperature and marine meteorological variables for the 20th century using ICOADS and the Kobe collection. Int J Climatol 25(7):865–879

Jiang W, Huang G, Huang P, Hu K (2018) Weakening of northwest pacific anticyclone anomalies during post-el niño summers under global warming. J Clim 31(9):3539–3555

Kay JE, Deser C, Phillips A, Mai A, Hannay C, Strand G, Arblaster JM, Bates S, Danabasoglu G, Edwards J et al (2015) The Community Earth System Model (CESM) large ensemble project: a community resource for studying climate change in the presence of internal climate variability. Bull Am Meteor Soc 96(8):1333–1349

Kobayashi S, Ota Y, Harada Y, Ebita A, Moriya M, Onoda H, Onogi K, Kamahori H, Kobayashi C, Endo H et al (2015) The JRA-55 reanalysis: general specifications and basic characteristics. J Meteorol Soc Jpn 93(1):5–48

Kripalani RH, Kulkarni A, Sabade S (2003) Western Himalayan snow cover and Indian monsoon rainfall: a re-examination with INSAT and NCEP/NCAR data. Theoret Appl Climatol 74(1):1–18

Kumar KK, Rajagopalan B, Cane MA (1999) On the weakening relationship between the Indian monsoon and ENSO. Science 284(5423):2156–2159

Lau N-C, Wang B (2006) Interactions between the Asian monsoon and the El Niño/Southern Oscillation: In The Asian Monsoon, pp. 479–512. Springer, Berlin, Heidelberg

Loschnigg J, Webster PJ (2000) A coupled ocean-atmosphere system of SST modulation for the Indian Ocean. J Clim 13(19):3342–3360

Mizuta R, Murata A, Ishii M, Shiogama H, Hibino K, Mori N, Arakawa O, Imada Y, Yoshida K, Aoyagi T et al (2017) Over 5,000 years of ensemble future climate simulations by 60-km global and 20-km regional atmospheric models. Bull Am Meteor Soc 98(7):1383–1398

Murray D, Hoell A, Hoerling M, Perlwitz J, Quan X-W, Allured D, Zhang T, Eischeid J, Smith CA, Barsugli J et al (2020) Facility for weather and climate assessments (FACTS): a community resource for assessing weather and climate variability. Bull Am Meteor Soc 101(7):1214–1224

Senan R, Orsolini YJ, Weisheimer A, Vitart F, Balsamo G, Stockdale TN, Dutra E, Doblas-Reyes FJ, Basang D (2016) Impact of springtime Himalayan-Tibetan Plateau snowpack on the onset of the Indian summer monsoon in coupled seasonal forecasts. Clim Dyn 47(9):2709–2725

Seth A, Giannini A, Rojas M, Rauscher SA, Bordoni S, Singh D, Camargo SJ (2019) Monsoon responses to climate changes-connecting past, present and future. Curr Clim Change Rep 5:63–79

Shaman J, Tziperman E (2005) The effect of ENSO on Tibetan Plateau snow depth: a stationary wave teleconnection mechanism and implications for the South Asian monsoons. J Clim 18(12):2067–2079

Takahashi HG (2011) Long-term changes in rainfall and tropical cyclone activity over South and Southeast Asia. Adv Geosci 30:17–22

Takahashi HG, Fujinami H (2021) Recent decadal enhancement of Meiyu-Baiu heavy rainfall over East Asia. Sci Rep 11(1):1–8

Takahashi HG, Yasunari T (2006) A climatological monsoon break in rainfall over Indochina-a singularity in the seasonal march of the Asian summer monsoon. J Clim 19(8):1545–1556

Takahashi HG, Yasunari T (2008) Decreasing trend in rainfall over Indochina during the late summer monsoon: impact of tropical cyclones. J Meteorol Soc Jpn 86(3):429–438

Takahashi HG, Watanabe S, Nakata M, Takemura T (2018) Response of the atmospheric hydrological cycle over the tropical Asian monsoon regions to anthropogenic aerosols and its seasonality. Prog Earth Planet Sci 5(1):1–14

Trenberth KE, Stepaniak DP, Caron JM (2000) The global monsoon as seen through the divergent atmospheric circulation. J Clim 13(22):3969–3993

Vernekar A, Zhou J, Shukla J (1995) The effect of Eurasian snow cover on the Indian monsoon. J Clim 8(2):248–266

Wang B, Li J, He Q (2017) Variable and robust east Asian monsoon rainfall response to el niño over the past 60 years (1957–2016). Adv Atmos Sci 34(10):1235–1248

Wang H, Xie S-P, Kosaka Y, Liu Q, Du Y (2019) Dynamics of Asian summer monsoon response to anthropogenic aerosol forcing. J Clim 32(3):843–858

Webster PJ, Yang S (1992) Monsoon and ENSO: selectively interactive systems. Q J R Meteorol Soc 118(507):877–926

Webster PJ, Magana VO, Palmer T, Shukla J, Tomas R, Yanai M, Yasunari T (1998) Monsoons: processes, predictability, and the prospects for prediction. J Geophys Res Oceans 103(C7):14451–14510

Wu T-W, Qian Z-A (2003) The relation between the Tibetan winter snow and the Asian summer monsoon and rainfall: an observational investigation. J Clim 16(12):2038–2051

Wu G, Liu Y, Zhang Q, Duan A, Wang T, Wan R, Liu X, Li W, Wang Z, Liang X (2007) The influence of mechanical and thermal forcing by the Tibetan Plateau on Asian climate. J Hydrometeorol 8(4):770–789

Wu G, Liu Y, He B, Bao Q, Duan A, Jin F-F (2012) Thermal controls on the Asian summer monsoon. Sci Rep 2(1):404

Xie S-P, Hu K, Hafner J, Tokinaga H, Du Y, Huang G, Sampe T (2009) Indian Ocean capacitor effect on Indo-western Pacific climate during the summer following El Niño. J Clim 22(3):730–747

Xie S-P, Kosaka Y, Du Y, Hu K, Chowdary JS, Huang G (2016) Indo-western Pacific Ocean capacitor and coherent climate anomalies in post-ENSO summer: a review. Adv Atmos Sci 33(4):411–432

Xue Y, Yao T, Boone AA, Diallo I, Liu Y, Zeng X, Lau WK, Sugimoto S, Tang Q, Pan X et al (2021) Impact of initialized land surface temperature and snowpack on subseasonal to seasonal prediction project, phase I (LS4P-I): organization and experimental design. Geoscientific Model Dev 14(7):4465–4494

Yanai M, Wu G-X (2006) Effects of the Tibetan Plateau: In: The Asian Monsoon, pp. 513–549. Springer, Berlin, Heidelberg

Yanai M, Li C, Song Z (1992) Seasonal heating of the Tibetan Plateau and its effects on the evolution of the Asian summer monsoon. J Meteorol Soc Jpn Ser II 70(1B):319–351

Yang S, Lau WK-M (2006) Interannual variability of the Asian monsoon: In The Asian Monsoon, pp. 259–293. Springer, Berlin, Heidelberg

Yasunari T (2006) Land-atmosphere interaction: In The Asian Monsoon, pp. 459–478. Springer, Berlin, Heidelberg

Yasunari T, Kitoh A, Tokioka T (1991) Local and remote responses to excessive snow mass over Eurasia appearing in the northern spring and summer climate -A study with the MRI-GCM-. J Meteorol Soc Jpn 69(4):473–487

Zhou W, Xie S-P (2018) A hierarchy of idealized monsoons in an intermediate GCM. J Clim 31(22):9021–9036